ENN Encyclopedia of Nanoscience and Nanotechnology
www.aspbs.com/enn

Localization and Interactions in Magnetic Nanostructures

F. G. Aliev
Universidad Autonoma de Madrid, Cantoblanco, Madrid, Spain

V. K. Dugaev
Max-Planck-Institut für Mikrostrukturphysik, Halle, Germany

J. Barnaś
Adam Mickiewicz University, Poznań, Poland

CONTENTS

1. Introduction
2. Early Experiments
3. Effects of Magnetic Field on the Localization Corrections
4. Electron–Electron Interaction in Spin Quantum Wells
5. Role of Spin–Orbit Interaction
6. Localization Corrections to the Anomalous Hall Effect
7. Interplay Between Localization and Band Magnetism
8. Localization Corrections Associated with Domain Walls
9. Localization Corrections to Magnetic Interactions in Multilayers
10. Localization Corrections to Spin Conductivity
11. Localization Effects in Low-Carrier-Density Magnets
12. Coulomb Interactions in Ferromagnetic Double Junctions
13. Transport Through Quantum Dots with Electron Correlations
14. Summary
Glossary
References

1. INTRODUCTION

One of the most spectacular phenomena discovered in recent years in magnetic artificially layered structures is the giant magnetoresistance (GMR) effect. The essence of the effect is the dependence of electrical resistance of a magnetic metallic multilayer on its magnetic configuration [1,2]. Such a configuration can be changed, for example, with an external magnetic field applied to the system. A typical structure in which the effect occurs is a multilayer with adjacent ferromagnetic films coupled antiferromagnetically across a nonmagnetic spacer [3,4] so that they have antiparallel magnetizations in the vanishing magnetic field. The magnetizations then rotate in an external field from the antiparallel configuration to the parallel one, and this rotation is accompanied by a decrease in the electrical resistance of the multilayer (an increase is also possible [5]). The effect exists for electric current flowing in the film plane [1,2,6], as well as for electric current flowing perpendicularly to the film plane [7–9]. The antiparallel alignment can also be obtained by other means. If, for instance, a multilayer consists of two types of ferromagnetic films (which have different coercive fields), then there is a range of magnetic fields during scan through the hysteresis loop where the magnetizations are antiparallel (being parallel above a certain saturation field) [6]. The GMR effect itself is a classical effect, and also exists at room temperature. Therefore, most of the experimental works on electronic transport in magnetic structures were done in this temperature range.

Whereas the transport properties of magnetic systems in the high-temperature regime are more interesting from

ISBN: 1-58883-060-8/$35.00
Copyright © 2004 by American Scientific Publishers
All rights of reproduction in any form reserved.

Encyclopedia of Nanoscience and Nanotechnology
Edited by H. S. Nalwa
Volume 4: Pages (587–605)

the application point of view, the low-temperature regime seems to be more interesting from the point of view of fundamental physics. This is because various quantum phenomena have peculiar contributions to transport characteristics, particularly in systems of reduced dimensionality. In such structures, usually one or more characteristic dimensions are in the nanometer range. When electrons propagate in a disordered system with the electron coherence length comparable to its (one or more) dimensions, the conductivity corrections due to quantum interference and electron–electron (e–e) interaction may play a significant role. Moreover, analysis of the phase-coherent effects in spin-polarized materials, particularly their dependence on the magnetic field and temperature, provides a sensitive way to investigate the degree and role of structural (morphological) and magnetic (domain walls) inhomogeneities. One may also expect that future spin electronics (spintronics) will take advantage of the phase-coherent transport in spin-polarized systems.

Localization effects in the transport properties of nonmagnetic metals and semiconductors were investigated very extensively during the last three decades, starting from the paper by Anderson [10]. The main results of these investigations have been summarized in several review articles [11–15]. The best developed seems to be the weak localization (WL) theory [11, 12], which gives a way to rigorously calculate localization corrections to the conductivity of disordered metals or degenerate semiconductors in the limit of $\varepsilon_F \tau/\hbar \gg 1$, where ε_F is the Fermi energy and τ is the momentum relaxation time of electrons. These corrections turn out to be strongly dependent on the temperature and magnetic field, and therefore they have been clearly observed in many experiments (see [15] for a review). The interaction theory of disordered systems [13, 14], which accounts for the quantum corrections to conductivity due to e–e interaction, has been developed in the same spirit as WL. Even though these two theories are constructed as perturbation theories, and thus are restricted to relatively small quantum corrections to conductivity, they explained a great number of experiments on disordered metals, heavily doped semiconductors, and amorphous metallic films. One of the most surprising properties of disordered systems is the effect of dimensionality in films and wires, and in small metallic particles. The essential point is that disordered systems are characterized by two characteristic lengths—the electron mean-free path l and the phase coherence length L_φ (or the Thouless length L_T in the interaction theory). The latter length scale corresponds to the distance at which the electron preserves its phase coherence, and this scale is associated with inelastic processes like scattering from phonons. When the geometrical size of a sample becomes smaller than L_φ, its transport properties are drastically changed since the quantum corrections for systems of different effective dimensionality are significantly different too. When the sample size is smaller than L_φ, the system is called *mesoscopic*. The origin of WL corrections to conductivity can be understood as a quantum effect due to the interference of electron waves propagating in a disorder potential [15, 16]. The quantum interference enhances the probability of an electron to return back to the starting point, which results in a tendency of the electron to localize. The external magnetic field and inelastic scattering from phonons suppress the quantum interference, which effectively decreases the magnitude of localization corrections. A different response of WL and e–e interaction to the magnetic field usually allows us to distinguish between the localization and e–e contributions [17]. The relevant theoretical formalism makes use of *diffusons* (particle–hole propagator) and *cooperons* (particle–particle propagator) [11, 12]. They describe propagation in space and time of the electron density and of the fluctuations of superconductive density, respectively. The effects of temperature, magnetic field, and spin–orbit (SO) interaction can be accounted for theoretically by considering the corresponding influence on the diffusons and cooperons.

The quantum corrections to conductivity due to WL and e–e interactions are usually limited to low temperatures. However, e–e interaction can lead to other phenomena, which in certain systems also have a significant influence on electronic transport at high temperatures. An example of such systems are tunnel junctions. Broad interest in magnetic tunnel junctions was initiated by successful applications of the GMR effect in read/write heads and magnetic field sensors [18]. Indeed, an effect qualitatively similar to GMR was also observed in magnetic tunnel junctions. Now, the junction resistance varies when the magnetizations of the ferromagnetic electrodes rotate from an antiparallel to a parallel alignment. The effect is commonly known as the tunnel magnetoresistance (TMR) effect, and was first observed in Co/Ge/Fe junctions by Julliere [19]. It results from the spin-dependent electronic band structure of the ferromagnetic electrodes and spin-dependent tunneling rates. The effect occurs not only in simple planar junctions [20], but also in more complex ones, like double magnetic junctions with ferromagnetic outer electrodes and magnetic or nonmagnetic central ones. In the latter case, the TMR effect in the sequential tunneling regime results from spin accumulation in the central electrode, which in turn is a consequence of spin-dependent tunneling rates across the barriers [21]. However, it also may occur in the coherent tunneling regime, where an electron is in a coherent state of the whole double-barrier system, and therefore is sensitive to the magnetic configuration of the outer electrodes.

In the case of double-barrier planar junctions, the central electrode (called also an island in the following) is sufficiently large to neglect the effects due to electrostatic interaction of an electron tunneling to this electrode with other electrons already being there. When the island becomes small, the electrostatic interaction of the excess electrons with the other ones may play a crucial role in electronic transport, leading to Coulomb blockade phenomena [22]. In asymmetric junctions, transport characteristics then form the well-known Coulomb staircase. Interplay of the charging phenomena and ferromagnetism of the electrodes [23] are briefly reviewed too.

The review then summarizes the results of experimental and theoretical studies of localization in ferromagnets, magnetic layers, and multilayers, as well as in mesoscopic

magnetic structures. It also includes recent results on the e–e correction to conductivity in disordered ferromagnetic structures, and the results on electrostatic charging effects in double magnetic junctions.

2. EARLY EXPERIMENTS

The low-temperature anomaly in electrical conductivity of ferromagnetic metals and thin films was reported in several experimental works. These works clearly demonstrate that the localization and interaction corrections to conductivity occur not only in nonmagnetic systems, but also in ferromagnets. However, interpretation of the results was not quite certain because the corresponding theory was not developed at that time. Here, we review some of these early experimental works. Kobayashi et al. [24] studied the temperature and magnetic field dependence of the electrical conductivity of highly resistive thin Ni films (film thickness of 40 and 60 Å). The samples were prepared in the following way [25, 26]. First, vacuum deposition of ferromagnetic metal (Ni of an amount which corresponded to 1 nm) onto quartz substrate was carried out, followed by oxidation at $6.5 \cdot 10^{-2}$ torr for a few minutes. At the next stage, this procedure was repeated two times with two more deposited Ni layers, each oxidized again. The resistance of the samples was controlled by changing the oxidation time. By analyzing electron micrographs, it was found that the film consisted of an ensemble of Ni nanoparticles with diameter of 1 nm (distribution of the size within ±5 Å) dispersed on the substrate. The stack of three layers of the particles formed a well-connected two-dimensional network of particles having only little overlap in the direction normal to the substrate. The third layer was covered with 50 nm thick SiO for protection. Kobayashi et al. [24] observed that the sheet conductivity $\Delta\sigma_\square \simeq [R_\square(T_0) - R_\square(T)]/R_\square^2(T_0)$ (here, $R_\square(T)$ is the sheet resistance) as a function of temperature has the form $\sigma_\square = \sigma_0 + A \ln T$. They also found the parameter A to be close to $e^2/(2\pi^2\hbar)$, and to be almost independent of the film thickness below 60 Å. Magnetoconductivity was positive, independent of temperature, and as small as 0.1% at 10 kOe. These results are in agreement with the WL theory in the effectively 2-D case. Some conclusions about the importance of spin–orbit (SO) interaction in ferromagnets were also drawn there.

The magnetoresistance (MR) of thin $Pd_{1-y}Ni_yH_x$ films of thickness 25, 50, and 100 Å was measured by Raffy et al. [27] between 1 and 5 K and in magnetic fields up to 1 T. With no hydrogen ($x = 0$) and for $y > 0.025$, the alloys are ferromagnetic, and display localization behavior in a zero magnetic field. Hydrogenation suppresses ferromagnetism in these materials, and for ($x \longrightarrow 1$), the ground state is dominated by magnetic fluctuations. It was shown that MR for 25 Å $Pd_{0.94}Ni_{0.06}H_x$ film could be fitted rather well by the 2-D form

$$\frac{\Delta R_\square}{R_\square^2} = \frac{e^2}{2\pi^2\hbar}(\beta - \alpha) Y\left(\frac{H}{H_0}\right) \tag{1}$$

where $Y(x) = \ln x + \psi(1/2 + 1/x)$, and $\psi(x)$ is the digamma function, which has the property $\psi(x) \simeq \ln(x)$ for $x \gg 1$ [28]. This is the formula for quantum correction in nonmagnetic metals, where the coefficient β is due to the Maki–Thompson correction [29] and α is due to the WL corrections, respectively, whereas H_0 is the phase-breaking field determined by spin-flip scattering and inelastic processes. MR was positive, and therefore accounted for by the suppression of the antilocalization correction in a magnetic field. The antilocalization effect was attributed to strong SO scattering. It should be noted that Pd and Ni alloys are close to the ferromagnetic transition at low temperatures. Introducing hydrogen into ferromagnetic Pd turns it into the paramagnetic state, whereas a relatively small concentration of Ni atoms leads to the presence of large-moment localized magnetic impurities or small magnetic clusters. The fact that the system is close to the phase transition point makes the interpretation of experimental results much more complex.

The resistivity of thin Fe films (for thickness above 60 Å) grown epitaxially on GaAs was studied by Fuller et al. [30] and Rubinstein et al. [31]. The iron films were grown on GaAs substrates by the molecular beam epitaxy (MBE) method. The substrate face orientation was chosen to be (110) in order to obtain within the film plane the following three different crystalline axes: the magnetically easy [001], hard [111], and intermediate [110] ones. It is known that epitaxial few monolayer Fe films can be obtained on MgO [32] and GaAs substrates [33, 34] because the corresponding nearest neighbor distances are close (within less than 1%) to that of bcc iron. The deposition of Fe on GaAs is of special importance because magnetic films deposited on semiconductors are important for application in spintronics. However, in this particular experiment on weak localization phenomena in Fe, specially prepared highly insulating substrates were used to allow studying transport properties of the iron films. These specially doped with chromium ($6 \cdot 10^{16}$ atoms · cm^{-3}) and tin ($2 \cdot 10^{16}$ atoms · cm^{-3}) GaAs substrates remained highly insulating, even when heated to 625 °C in a vacuum for about 30 min. Several samples, grown with thicknesses from 60 to 200 Å, were photolitographically patterned to three conducting stripes, aligned along one of three different magnetic axes: easy, intermediate, and hard. The temperature dependence shows a shallow minimum at approximately 15 K, and at lower temperatures, obeyed the log law $\sigma_\square = \sigma_0 + A \ln T$, with the coefficient A very close to $e^2/(2\pi^2\hbar)$ [30, 31]. It was shown that the anomalous temperature dependence did not vary with the current and sample orientation [31]. This temperature dependence was not affected by magnetic fields up to 600 G. A small negative MR was observed only at magnetic fields larger than 30 kG. No anomaly in the low-temperature conductivity was observed for films of thickness larger than 100 Å, which excludes the Kondo effect as a possible explanation of the experimental results. A comparison of the temperature dependence of the resistivity and of the normal Hall effect did not allow to distinguish between the interaction and WL corrections, mainly because of the experimental error. Finally, at 4.2 K, the high-field MR appeared to be negative, and varying linearly with the magnetic field between 30 and 130 kG. This is inconsistent

with the e–e interaction and WL theories, which predict the $\ln H$ and $-\ln H$ dependence in this regime, respectively.

Aprili et al. [35] measured the low-temperature conductivity of inhomogeneous Ni films near the percolation threshold. Homogeneous layers of thickness $d = 6$ nm were first evaporated using electron guns in ultra high vacuum (10^{-9} torr). Percolating Ni films were prepared by controlled coalescence due to the annealing of homogeneous films at temperatures from 500 to 550 °C in ultrapure He vapor. The annealing process was controlled by resistance measurements, which provided an accurate method for following the evolution of the inhomogeneous state. Moreover, the annealing allowed a reduction of the amount of atomic size effects, leading to relatively large-scale topological disorder only. The metallic coverage (p) was deduced by analyzing transmission electron microscopy images after annealing. A percolation coverage of about $p_c = 0.56$ and a fractal dimensionality $d_f = 1.8$ were found to be in good agreement with theoretical predictions [35]. Assuming the diffusion coefficient $D = 5 \cdot 10^{-4}$ $m^2 \cdot s^{-1}$, found in Ni-based percolation alloys [27], the authors estimated that, for temperatures below 30 K, the scale on which the phase coherence is preserved, $L_T = \sqrt{D\hbar/k_B T}$, should become larger than a typical film thickness, indicating possible two-dimensional quantum transport. Indeed, the $\log T$ anomaly was found experimentally, which was well fitted with the formula $\Delta\sigma_\square = (e^2/2\pi^2\hbar)[1 + 2(1 - F)] \log T - K_d T^\alpha / dR_\square$, where the first two terms account for quantum transport (WL contributes to the coefficient 1 and e–e interaction to the factor $2(1 - F)$, F being a screening factor). The second term reflects ordinary inelastic scattering with K_d, the coupling coefficient. It was also observed that the external magnetic field of 4 T did not affect $\Delta\sigma_\square(T)$, indicating that the quantum correction was mainly due to e–e interaction in 2-D. Moreover, from the $\log T$ fit, one can obtain $F = 0.55$, which was close to the screening factor of 0.53 estimated theoretically. For percolating films, the logarithmic slope was found to be partially suppressed. Moreover, a signature of a modified dimensionality at $T < 4$ K was reported, reflecting the transition to the regime, where the phase-coherent scale becomes close to the percolation length. Magnetoresistivity measurements performed by subtracting data obtained at 20 K (i.e., in the classical regime) showed that some contribution due to WL is also present. The dependence of a small additional (positive) contribution to the conductivity on the external magnetic field became logarithmic at high fields (above 3 T), and can be approximated by formula (1).

3. EFFECTS OF MAGNETIC FIELD ON THE LOCALIZATION CORRECTIONS

An analysis of the localization corrections in ferromagnetically ordered metals or semiconductors was carried out in [36–38], where the results were also compared to the corresponding ones derived for nonmagnetic materials [11,12]. It was shown that there were two main sources which affect the localization corrections: the internal induction $\mathbf{B}$ and the magnetization field $\mathbf{M}$. For theoretical analysis [36–38], a model described by the following Hamiltonian

$$H = -\frac{\hbar^2}{2m}\left(\frac{\partial}{\partial \mathbf{r}} - \frac{ie\mathbf{A}}{\hbar c}\right)^2 - \mathbf{M}\cdot\boldsymbol{\sigma} \tag{2}$$

was used, where the vector potential $\mathbf{A}$ is related to the magnetic induction $\mathbf{B}$ by $\mathbf{B} = \mathrm{rot}\,\mathbf{A}$, $\mathbf{M}$ has the dimensionality of energy, and $\boldsymbol{\sigma}$ is the vector of Pauli matrices. The first term in Eq. (2) describes electrons moving in the magnetic field $\mathbf{B}$, whereas the second one takes into account the Zeeman splitting of spin-up and spin-down electron bands. Both factors in the Hamiltonian affect the localization corrections. It is known that the first term suppresses the cooperons, whereas the second one suppresses singlet cooperons and singlet diffusons [11,12]. In good metallic ferromagnets, the magnitude of the spin-splitting M related to the second term of Eq. (2) is of the order of Fermi energy ε_F. On the other hand, there is a general condition, $\varepsilon_F\tau/\hbar \gg 1$, on which the WL theory is valid (i.e., when the localization corrections can be considered as small corrections). Therefore, one can assume that, in good ferromagnetic metals, the condition $M\tau/\hbar \gg 1$ is also fulfilled. It can be shown [37] that when this condition is fulfilled, the contribution of singlet diffusons and cooperons can be neglected. Bearing this in mind, one can find the localization corrections to conductivity by direct generalization of the results derived for nonmagnetic metals [11,12].

In the three-dimensional case, the localization correction to the conductivity, which includes only triplet cooperons and takes into account the magnetic induction B, can be written in the following form:

$$\Delta\sigma(B) = \Delta\sigma(0) - \frac{e^2}{16\pi^2\hbar l_B} \times \sum_{n=0}^{\infty}\left[\frac{1}{(n+1/2+\delta_\uparrow)^{1/2}} - 2(n+1+\delta_\uparrow)^{1/2} + 2(n+\delta_\uparrow)^{1/2} + \frac{1}{(n+1/2+\delta_\downarrow)^{1/2}} - 2(n+1+\delta_\downarrow)^{1/2} + 2(n+\delta_\downarrow)^{1/2}\right] \tag{3}$$

where $\sigma(0)$ does not include the effects due to magnetic induction, and is given by

$$\Delta\sigma(0) = C + \frac{e^2}{4\pi^2\hbar}\left[\frac{1}{D_\uparrow^{1/2}}\left(\frac{1}{\tilde{\tau}_{so\uparrow}} + \frac{1}{\tau_{\varphi\uparrow}}\right)^{1/2} + \frac{1}{D_\downarrow^{1/2}}\left(\frac{1}{\tilde{\tau}_{so\downarrow}} + \frac{1}{\tau_{\varphi\downarrow}}\right)^{1/2}\right] \tag{4}$$

with the following notations introduced:

$$C \simeq -\frac{e^2}{2\pi^2\hbar l}, \qquad \delta_{\uparrow(\downarrow)} = \frac{l_B^2}{4D_{\uparrow(\downarrow)}}\left(\frac{1}{\tilde{\tau}_{so\uparrow(\downarrow)}} + \frac{1}{\tau_{\varphi\uparrow(\downarrow)}}\right) \tag{5}$$

Here, $D_{\uparrow(\downarrow)} = v_{F\uparrow(\downarrow)}^2 \tau_{\uparrow(\downarrow)}/3$ are the diffusion coefficients, and $v_{F,\uparrow(\downarrow)}$ are the Fermi velocities for spin-up and spin-down electrons. Apart from this, $l_B = (c\hbar/eB)^{1/2}$ is the magnetic length, and l is the electron mean-free path. Spin–orbit

interaction is included, and is described by the SO relaxation time of cooperons $\tilde{\tau}_{so\uparrow(\downarrow)}$ and the phase relaxation time $\tau_{\varphi\uparrow(\downarrow)}$, related to the inelastic scattering of electrons from phonons. The dependence of τ_φ on T results in the temperature dependence of conductivity at low T. Formula (3) was found by Kawabata's method [39], and is limited to weak magnetic induction, when $l_B \gg l$. The magnetoresistivity is found to be *negative* due to the suppression of the negative localization correction by magnetic induction **B**. In the case of $l_B < l$, the localization correction vanishes, being completely suppressed by the magnetic induction. At $\delta_\uparrow, \delta_\downarrow \ll 1$ (i.e., for low temperatures or strong magnetic induction), the sum in Eq. (3) is a constant $C_2 = -0.13$ [39], which leads to the $\sqrt{B}$ dependence of the localization correction on B. In the opposite limit of weak magnetic induction, one has $\delta_\uparrow, \delta_\downarrow \gg 1$, and the correction is proportional to B^2. The derived formulas describe the dependence on the total magnetic induction, which in turn depends on the external magnetic field.

In the effectively 2-D case, the localization correction has the form

$$\Delta\sigma(B) = -\frac{e^2}{4\pi^2\hbar}\left[\psi\left(\frac{1}{2}+\frac{1}{\tau_\uparrow a_\uparrow}\right) - \psi\left(\frac{1}{2}+\frac{1}{\tilde{\tau}_{so\uparrow}a_\uparrow}+\frac{1}{\tau_{\varphi\uparrow}a_\uparrow}\right) + \psi\left(\frac{1}{2}+\frac{1}{\tau_\downarrow a_\downarrow}\right) - \psi\left(\frac{1}{2}+\frac{1}{\tilde{\tau}_{so\downarrow}a_\downarrow}+\frac{1}{\tau_{\varphi\downarrow}a_\downarrow}\right)\right] \quad (6)$$

where $a_{\uparrow,\downarrow} = 4eBD_{\uparrow,\downarrow}/c\hbar$. In the limit of $B \to 0$, the localization correction has a form similar to that in the nonmagnetic case:

$$\delta\sigma(0) = \frac{e^2}{4\pi^2\hbar}\ln\left[\tau_\uparrow\tau_\downarrow\left(\frac{1}{\tilde{\tau}_{so\uparrow}}+\frac{1}{\tau_{\varphi\uparrow}}\right)\left(\frac{1}{\tilde{\tau}_{so\downarrow}}+\frac{1}{\tau_{\varphi\downarrow}}\right)\right] \quad (7)$$

In both effective 3-D and effective 2-D cases, the localization correction to conductivity is *negative*, and the magnitude of this correction decreases with increasing **B**. The latter takes into account both the internal magnetic induction and the effect of the external magnetic field. Thus, the localization can be observed only in the case of a weak suppression of the localization correction by the internal induction.

The key question for quantum corrections is: how long is the phase coherence length? Tatara and Barbara [40] theoretically considered the Aharonov–Bohm effect in a disordered ferromagnetic ring. The Aharonov–Bohm effect is a macroscopic manifestation of the quantum interference of electron waves. It shows up as oscillations of electric current in a small metallic ring as a function of the external magnetic field. In the case of superconductors or pure nonmagnetic metals, the oscillation factor in the dependence of electric current on the magnetic field is known to be $\cos(2\pi\phi/\phi_0)$, where ϕ is the magnetic flux penetrating through the ring, and $\phi_0 = hc/e$ is the magnetic flux quantum. The corresponding theory for disordered normal metals was developed by Altshuler et al. [41], and it was shown that, in disordered metals, the corresponding factor should be $\cos(4\pi\phi/\phi_0)$ instead of $\cos(2\pi\phi/\phi_0)$. This is because the cooperon contributing to the current in the ring carries the double electron charge $2e$, and therefore the effective magnetic quantum is half of the usual value hc/e. The theoretical prediction of [41] was later confirmed in experiments with gold rings [42]. Due to the internal magnetization and internal induction in ferromagnets, the Aharonov–Bohm effect was shown [40] to be different from the analogous effect in nonmagnetic disordered metallic rings. The main difference is related to the influence of magnetization on the components of the cooperon. Each spin component contributes to the Aharonov–Bohm effect, with a damping factor depending on the scattering of electrons in each spin channel. Due to the possibility of a large difference in the mean-free paths of spin-up and spin-down electrons, only electrons of a specific spin orientation contribute to the effect. Thus, ferromagnetism does not suppress the Aharonov–Bohm effect, even if the difference in the spin-up and spin-down relaxation times is large (as, for example, in Fe).

Aliev et al. [43] measured MR of 17 nm thick Co wires with a width of 200 nm and a length of 1 μm at temperatures from 4 K down to 100 mK, and in magnetic fields up to 15 T perpendicular to the structure. The polycrystalline wire structures were grown at room temperature by molecular beam epitaxy, followed by electron lithography patterning. Electric measurements were performed in a dilution He^3–He^4 refrigerator by using the standard ac bridge technique (LR700), which assured low dissipation at low temperatures. The low-temperature resistivity (30 $\mu\Omega \cdot$ cm) confirmed the polycrystalline structure of the sample, and indicated that the elastic mean-free path was slightly smaller than the strip cross-section dimensions. Figure 1 presents the data obtained at 100 mK at different values of electric currents between 10 and 1 μA, and for magnetic fields well outside the region where the anisotropic MR (AMR) could affect the results. One can clearly see reproducible conductance fluctuations with an amplitude of the order of $0.01e^2/h$ at the lowest currents and temperatures. Strong suppression of the resistance fluctuations with the current above 10 μA and temperature $T > 4$ K indicates that these anomalies are not induced by a reproducible rearrangement of the internal magnetic structure. These conductance fluctuations also indicate the phase-coherent transport.

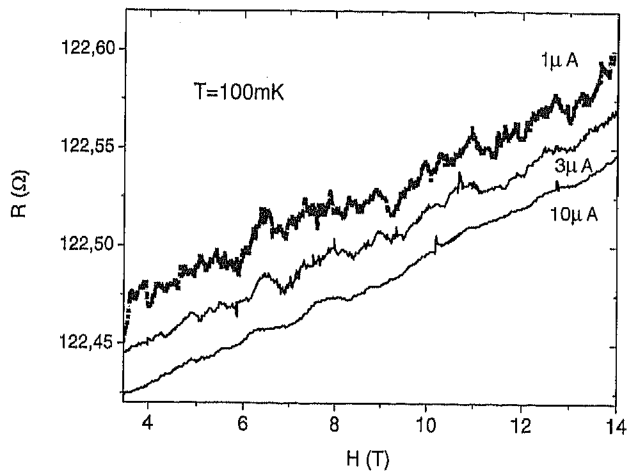

Figure 1. Reproducible magnetoresistance fluctuations in 17 nm thick Co line structures with width of 200 nm and length 1 of μm observed at ultralow temperatures (100 mK) at different electric currents from 10 to 1 μA.

Recently, Kasai et al. [44] observed the Aharonov–Bohm effect in a ferromagnetic permalloy nanoring. The sample consisted of a nanoscale ring with leads made of permalloy ($Fe_{19}Ni_{81}$) and patterned by using the lift-off technique and electron-beam lithography. First, a thin photoresist of 100 nm was spin coated onto a thermally oxidized Si substrate. The resist mask was then patterned with a 20 keV electron beam. After development, permalloy was deposited by an electron-beam evaporator with 0.5 nm/s. The sample was then obtained after the resist mask had been lifted off in solvent. A scanning electron microscope was used to image and determine the dimensions of the sample. For resistance measurement, Cu electrodes were attached to the leads. The distance between the two voltage electrodes was 2.5 μm. The outer and inner diameters were, respectively, equal to 500 and 420 nm, whereas the thickness was 20 nm. The magnetoresistivity of the ring was measured from 30 mK to 4 K in a magnetic field perpendicular to the ring plane. For magnetic fields large enough to exclude AMR, the authors [44] observed aperiodic fluctuations and periodic resistance oscillations. The aperiodic fluctuations, similar to those found for Co line structures [43], have been identified as being due to the universal conductance fluctuations. By calculating the power spectrum from the Fourier transform of the MR data obtained in the range from 3 to 4 T, it was concluded that the Aharonov–Bohm oscillations had a period $\Delta B =$ 0.0266 T, which was consistent with the estimated range of $0.0209T < \Delta B < 0.0299T$, given by the inner and outer diameters of the ring. The oscillation period was found to be dependent on the magnetic field tilting angle. The amplitude of oscillations was estimated to be about $0.001e^2/h$, which was almost three orders of magnitude smaller than one might expect for the fully phase-coherent diffusive conductor. The reduced value of the conductance oscillations was explained by a small (as compared to paramagnetic metals) phase-coherence length (500 nm). In ferromagnets, the phase-coherence length is significantly reduced by spin-flip scattering.

4. ELECTRON–ELECTRON INTERACTION IN SPIN QUANTUM WELLS

Contrary to WL, the e–e interaction corrections in ferromagnets are not suppressed by the internal magnetic induction. This is because the interaction corrections are described mainly by the diffusons, which are not affected by the magnetic induction. The main difference between nonmagnetic and ferromagnetic metals, as concerns the interaction corrections, is the suppression of the contribution due to singlet diffusons. Thus, taking into account only triplet diffusons, one finds the following form for the exchange term in the interaction correction [36, 38]:

$$\Delta\sigma_{ex} = \frac{e^2}{2\pi^2\hbar(\nu_\uparrow + \nu_\downarrow)}\left[\nu_\uparrow \ln\left(\frac{T\tau_\uparrow}{\hbar}\right) + \nu_\downarrow \ln\left(\frac{T\tau_\downarrow}{\hbar}\right)\right] \quad (8)$$

where $\nu_{\uparrow(\downarrow)}$ is the density of states of spin-up (down) electrons at the Fermi level, and T is taken in the energy units. The Hartree term in the correction, on the other hand, is given by the formula

$$\Delta\sigma_{\rm Har} = -\frac{e^2}{4\pi^2\hbar}\left[F_\uparrow \ln\left(\frac{T\tau_\downarrow}{\hbar}\right) + F_\downarrow \ln\left(\frac{T\tau_\downarrow}{\hbar}\right)\right] \quad (9)$$

The above expression contains the constants $F_\uparrow$ and $F_\downarrow$, which are determined by the average ratio of the Coulomb interaction matrix elements with the momentum k to the matrix element with $k = 0$ [13, 12]. Here, k is the momentum transferred due to e–e interaction for the electrons at the Fermi surface. The difference between $F_\uparrow$ and $F_\downarrow$ is due to the different Fermi surfaces of spin-up and spin-down electrons.

Experimentally, the interaction corrections to the conductivity were observed by Aliev et al. [45] in Co/(Cr/Ag)/Co multilayers. The multilayers were prepared on MgO(100) substrates in a molecular beam epitaxy (MBE) deposition system using electron-beam guns and a mass spectrometer control system to stabilize the growth rate. In order to vary the thickness systematically, the Cr and Ag films were grown in a wedge shape. Then the system was cut into long stripes. The following multilayer composition was studied: Co(45 Å)/Cr(0–15 Å)/Ag(0–20 Å)/Co(45 Å), covered by 20 Å of Ag as a protection layer. The sample surface and structure were studied in detail by atomic force microscopy (AFM), X-ray diffraction (XRD), and magnetic force microscopy (MFM) [45]. The AFM measurements on the thinnest part of the wedge gave an rms roughness of 0.4 nm over a $2.5 \cdot 2.5$ μm^2 area, while for the thickest part of the wedge, an rms roughness of 1.5 nm was obtained for the same area. The average grain diameter observed using AFM images was 50 nm. Low-angle specular XRD spectra clearly showed a series of well-defined finite-size oscillations, again an indication of low film roughness. The temperature dependence of conductivity at $T < 20$ K shows the logarithmic dependence on T, fitted by the formula $\rho = A \log T + C$ (see Fig. 2). Possible reasons for the observed logarithmic increase of the resistivity at low temperatures could be: (1) the Kondo effect, (2) WL effects, (3) disorder-enhanced two-dimensional e–e interactions, or (4) the interaction of conduction electrons with two-level systems. The first two effects are sensitive to low magnetic fields, and give rise to negative MR. They can be distinguished from the other interactions by applying a sufficiently strong magnetic field. The estimated upper limit for the Kondo temperature was $T_K = 7$ K, defined as the middle point of the temperature interval, where the resistivity grows logarithmically. Therefore, for the usual Kondo effect, the temperature dependence of the resistivity should be substantially changed by the field $H = 110$ kG. Characteristic fields which suppress WL effects are usually lower than 1 kG. However, it was found [45] that even the magnetic field of 110 kG had almost no influence on the logarithmic slope. The lack of saturation of the resistivity down to ultralow temperatures, both for $H = 0$ and in the magnetic field of 110 kG, implies that the logarithmic term in the resistivity is likely due to the 2-D type e–e interactions in the presence of disorder. However, the experimental data [45] do not allow to exclude some additional contribution to the resistivity due to scattering on two-level systems. The indication of such a possibility comes

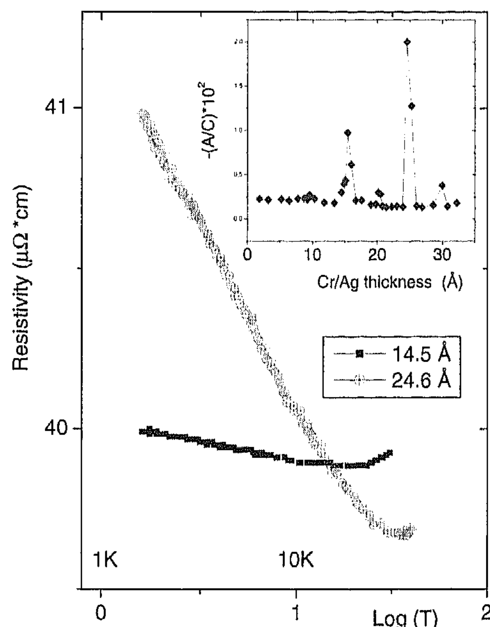

Figure 2. Logarithmic dependence of resistivity at $T < 20$ K ($\rho = A \cdot \log T + C$) for two Co (45 Å)/(Cr/Ag)/Co (45 Å) trilayers with different thicknesses of Cr/Ag spacer. Inset shows plot ($-A/C$) as a function of the Cr/Ag spacer thickness.

from the deviation from the log-T behavior in the resistivity at ultralow temperatures [46].

The thickness dependence of the observed normalized logarithmic term in the resistivity, A/C, was found to be rather unusual (see the inset in Fig. 2). For the elastic scattering times 10^{-9}–10^{-13} s within an accuracy of 0.01, the ratio A/C in the log-T fit is proportional to the product of the e–e interaction coefficient F and the residual resistivity [45]. For all studied strips, the coefficient F turned out to be strongly dependent on the thickness L of the (Cr/Ag) spacer layer. At some values of L, however, resonance-like peaks of F were observed. An explanation of this intriguing observation, given by Aliev et al. [45], was related to a change of disorder at the Cr/Ag interface with increasing thickness of the Cr/Ag spacer. The observed periodicity of 5 Å indeed corresponds roughly to 2.1 Å for Cr and 2.9 Å for Ag. An atomic monolayer of Cr in the preferential (110) direction is around 2.04 Å thick, which is in good agreement with the 2.1 Å estimated above. It is worth noting that interface-morphology-induced oscillations with a one monolayer periodicity also were observed in the magnetic properties and in the in-plane lattice spacing of cobalt [47–49] and gold ultrathin films [50].

Another possible explanation of this phenomenon is based on the screening effects in spin-separated quantum wells created by the multilayer structure [36]. In a simplified model, one may assume two different quantum wells, respectively for spin-up and spin-down electrons. Correspondingly, there are two different spin channels for the localization corrections. The coupling constant of e–e interaction is also associated with each of the spin channels. However, the screening of e–e interaction may include electrons with both spin orientations, provided that the corresponding matrix elements obey certain selection rules. The resonance effect occurs when the ratio of the spin-up and spin-down quantum well widths is an integer. Physically, this corresponds to a commensurability of the wavefunctions of electrons with different spin orientations.

5. ROLE OF SPIN–ORBIT INTERACTION

The SO interaction plays an important role in the localization phenomena. It is well known that, in nonmagnetic metals, the presence of SO interaction can change the sign of the localization correction. As a result, the low-temperature conductivity of metals with strong SO interactions increases with decreasing temperature, what is known as the weak antilocalization effect. The change of the sign of localization correction is associated with the suppression of triplet cooperons by the SO interaction. In nonmagnetic metals, there are contributions from singlet and triplet cooperons, which have different signs and which enter with coefficients reflecting the multiplicity of the corresponding states: $+1$ for the singlet and -3 for the triplet [13, 12]. Without SO interaction, this results in a negative correction since each component of the triplet gives the same contribution as one component of the singlet. By switching on a sufficiently strong SO interaction, one suppresses the triplet cooperon, and only the singlet cooperon is then relevant. This results in the sign reversal of the localization correction.

The situation is different in ferromagnetic metals, where the relatively strong internal magnetization completely excludes the singlet cooperons. Thus, the localization correction is negative, that is, there is no weak antilocalization. On the other hand, the SO interaction affects the triplet cooperons, decreasing the localization correction, making it smaller than in nonmagnetic metals. That is why the SO interaction is of main importance for the localization corrections in ferromagnets.

The SO interaction occurs as a relativistic effect in electron scattering from impurities and defects. It also occurs as the Rashba terms due to the interfaces [51], and the Dresselhaus terms [52] due to the higher order k terms in the electron Hamiltonian. The effects of SO interaction on the cooperons, related to the scattering from impurities and to the Rashba terms, have been studied theoretically in the case of bulk and effectively 2-D ferromagnets [37]. The most important result is that the SO interaction entering the cooperons turns out to be strongly dependent on the orientation of magnetization vector **M** in 2-D structures. More precisely, the inverse SO relaxation time $\tilde{\tau}_{so}^{-1}$ vanishes when the magnetization is in the plane of the layers.

It is worth noting that the SO interaction should be even more pronounced in the case of multilayered structures than in single films. As we pointed out before, the potential steps at the interfaces in combination with the relativistic terms in the Hamiltonian may produce strong SO scattering. The corresponding theory for the interface SO interaction was proposed by Bychkov and Rashba [51]. In the case of Fe/Cr multilayers, the potential steps are about 2.5 eV for the majority of electrons, and one can expect a significant SO scattering from the interface.

6. LOCALIZATION CORRECTIONS TO THE ANOMALOUS HALL EFFECT

Theoretical and experimental investigation of the anomalous (or extraordinary) Hall effect (AHE) in ferromagnets has a long history [53]. Recently, this effect has attracted much interest because it can be used to determine the magnitude and orientation of the magnetization in some magnetic materials, structures, and devices. AHE can be measured as a Hall voltage induced by an electric current flowing in the direction perpendicular to the magnetization **M**. In contrast to the usual Hall effect, AHE does not require any external magnetic field. Two different mechanisms leading to AHE have been studied thoroughly: the so-called *side-jump* and *skew-scattering* mechanisms. They both essentially involve the SO interaction. The physical reason for AHE is a spin-dependent lateral displacement of the electron wave packet during the scattering from impurity (side jump) and a spin-dependent anisotropy of the scattering amplitude (skew scattering) [54].

The calculation of the off-diagonal conductivity σ_{xy} in a ferromagnet can be performed using the diagram technique. Considering a loop diagram with the SO correction to the vertex part (this is the side-jump mechanism), Crépieux and Bruno [54] found the following formula for σ_{xy}:

$$\sigma_{xy}^{(sj)} = \frac{e^2\lambda_0^2}{6}(\nu_\downarrow k_{F\downarrow} v_{F\downarrow} - \nu_\uparrow k_{F\uparrow} v_{F\uparrow}) \tag{10}$$

where $k_{F\uparrow,\downarrow}$, $v_{F\uparrow,\downarrow}$, and $\nu_{\uparrow,\downarrow}$ are the electron momentum, electron velocity, and the density of states for spin-up and spin-down electrons at the Fermi surfaces. The constant λ_0 measures the strength of the SO interaction. It has the dimensionality of length, and for nonrelativistic electrons in vacuum, $\lambda_0 = \lambda_c/2\pi$, where $\lambda_c = 2\pi\hbar/m_0c$ is the Compton wavelength of electrons and m_0 is the free electron mass. The magnitude of λ_0 in crystals is changed due to crystalline fields.

Within the skew-scattering mechanism, one takes into account the loop diagrams with the third-order corrections due to scattering from impurities, keeping the first order in SO interaction [54]. The result of relevant calculation is

$$\sigma_{xy}^{(ss)} = \frac{\pi\langle V^3\rangle\lambda_0^2 a_0^3}{6\langle V^2\rangle}[\sigma_{xx,\downarrow}k_{F\downarrow}^2\nu_\downarrow - \sigma_{xx,\uparrow}k_{F\uparrow}^2\nu_\uparrow] \tag{11}$$

where $\sigma_{xx,\uparrow,\downarrow}$ are the diagonal conductivities in the spin-up and spin-down channels, and a_0 is the lattice parameter. Here, V measures the amplitude of disorder, and the angle brackets mean averaging over disorder. The dimensionless ratio $\langle V^3\rangle/\langle V^2\rangle^{3/2}$ depends only on the distribution $P(V)$ of the random field $V(\mathbf{r})$, whereas $\nu a_0^3\langle V^2\rangle^{1/2}$ characterizes the relative strength of the potential.

Localization correction to the anomalous Hall effect has been studied experimentally on several amorphous ferromagnetic Fe films with thickness from two to ten atomic layers [55]. The films were prepared *in-situ* by quenched condensation onto a crystalline quartz substrate held at helium temperature in a vacuum better than 10^{-11} torr. Homogeneous amorphous iron films of less than two monolayers thickness could be obtained by this method if they were deposited on an insulating Sb buffer layer with a thickness of ten monolayers. An additional indication on the amorphous structure of the films was the resistively detected irreversible transformation to the crystalline state for films of thickness of more than 18 monolayers, when they were heated to above 40 K. Details of the sample preparation are described in [56]. It has been found [55] that the quantum correction to the off-diagonal (Hall) conductance $\Delta\sigma_{xy}$ is negligibly small in the low-temperature region, in which the correction to the conductance $\Delta\sigma_{xx} \sim \log T$ is clearly seen. In other words, the quantum corrections due to localization and e–e interaction to the off-diagonal conductance vanish in ferromagnetic films. This result is in contrast to what is known of the localization corrections to the usual Hall effect [11, 12], for which the localization correction to the off-diagonal conductance is nonzero, and this exactly compensates the effect of localization correction in diagonal conductance for the Hall constant. As a result, the localization correction to the Hall constant is exactly zero, but the correction to σ_{xy} is not zero. The theoretical analysis for ferromagnets has been done in [57–60]. It was shown that the results are different for different mechanisms of AHE. Namely, the localization correction to σ_{xy} is nonzero for the skew scattering [57, 58], but it vanishes for the side-jump mechanism [58]. In the latter case, exact cancellation of the contributions from different diagrams takes place. In addition, the exchange interaction correction for the skew-scattering mechanism was shown to vanish too [57]. Thus, the experiment of Bergmann and Ye [55] can be interpreted either as the localization correction strongly suppressed by the SO interaction within the skew scattering [57], or as the localization correction within the side-jump mechanism [58]. The latter interpretation is better justified for an alloy-like type of disorder described by the Gaussian distribution of random fields. Such a type of disorder (alloys, amorphous systems) is in contrast to the impurity disorder (doped semiconductors).

7. INTERPLAY BETWEEN LOCALIZATION AND BAND MAGNETISM

The above discussion of the WL and e–e interaction corrections to conductivity applies to systems far from the critical point of ferromagnetic transition, where the magnetic fluctuations are very weak. An important issue is the influence of localization on the magnetic ordering in itinerant ferromagnets. This effect should be of key importance near the critical point, where the magnetic fluctuations are affected by the localization effects. In other words, magnetic fluctuations, cooperons, and diffusons should be considered at the same footing. This problem was studied in [61, 62]. Fukuyama [61] considered a ferromagnet in the framework of the Hubbard model and in the presence of random short-range impurities. He found that the Curie temperature T_c depends substantially on the disorder which leads to an increase in T_c. The reason for this is that the Coulomb interaction leading to ferromagnetism is effectively enhanced due the to the diffusive motion of electrons.

A similar model, with two coupling constants describing the Hubbard interaction in a disordered electron system, was studied by Singh and Fradkin [62]. They found that the effect of enhancement of the e–e interaction by the localization can be so strong that the electrons can be localized, and

at the same time, the ferromagnetic ordering can persist. The authors called such a system the *ferromagnetic Anderson insulator*. The other important aspect of the self-consistent calculation in their work was *no suppression of the singlet cooperon* by the spontaneous magnetization. This resulted from an interplay of different types of fluctuations in the vicinity of the magnetic phase transition point.

Recently, Kim and Millis [63] predicted a singular renormalization of the amplitude of backscattering from impurities, when the correlation length near the ferromagnetic magnetic quantum critical point exceeds the mean-free path. In other words, long wavelength fluctuations may dramatically increase the backscattering by spinless impurities. This effect leads to an enhancement of the Altshuler–Aronov correction to conductivity from $\log(1/T)$ to $\log^2(1/T)$. Besides, peculiar Friedel oscillations in the electron density near the impurities should occur for a magnetic-field-induced quantum-phase transition. Due to a nonzero magnetic field, the spin-up and spin-down Fermi surfaces are characterized by different wavevectors. Accordingly, two superimposed oscillations in the electron density may be expected near any impurity.

On the experimental side, localization effects due to the magnetically tuned quantum-phase transition were observed in synthetic antiferromagnet (Fe/Cr) [64] and natural quasi two-dimensional metal $Sr_3Ru_2O_7$ [65]. The ruthenate $Sr_3Ru_2O_7$ is the $n = 2$ member of the series of layered perovskites $Sr_{n+1}Ru_nO_{3n+1}$. The end members of the series are the pseudocubic and itinerant ferromagnet $SrRuO_3$ ($n = \infty$) [66] and the strongly two-dimensional unconventional superconductor Sr_2RuO_4 [67]. The high-quality single crystals were grown using methods described in [68]. It was found that critical fluctuations near the metamagnetic phase transition in quasi two-dimensional metal $Sr_3Ru_2O_7$ strongly enhance the residual resistivity ρ_{res} as the temperature is lowered below a few kelvin [65]. The low-temperature resistivity, however, varies as $\rho = \rho_{res} + AT^{\alpha}$, with $\alpha \simeq 1$. Similar conclusions have been drawn from the study of the magnetic-field-tuned quantum-phase transition in antiferromagnetically coupled Fe/Cr multilayers (see the next section and [64] for details of the sample growth and characterization). The difference is that, in the latter case, the maximum in the residual resistivity is overshadowed by a strong magnetic-field-dependent resistance, that is, by the GMR effect.

8. LOCALIZATION CORRECTIONS ASSOCIATED WITH DOMAIN WALLS

It has been known for a long time that magnetic domain walls (DWs) contribute to MR (DWMR). Electron transport through a narrow DW is predominantly ballistic [69], whereas for thick DWs it is rather diffusive. In the latter case, the quantum corrections due to WL and e–e interaction in the presence of disorder can also play a significant role, leading to interesting MR phenomena [70–72]. Recent interest in the DW contribution to resistivity is stimulated by intriguing physics which underlies the DWMR effect [73–77], and also by possible applications. Indeed, DWs can have a significant influence on the electrical noise and operation of magnetoelectronic devices [78]. Although the number of DWs was controlled and directly observed, for example, in Fe [77] and Co films [75] at room temperature, where DW formation is relatively well understood, no clear picture emerged which could allow an understanding of the results. AMR dominates the low-field MR, and complicates the extraction of the true DW contribution to the resistivity [79]. In order to minimize the AMR contribution, thin films with reduced magnetization and special DW configurations have been studied [80].

The localization corrections in the presence of DWs are affected by a specific perturbation, which can be described as an effective gauge field arising in the vicinity of DWs. This problem has been studied theoretically in several works [70–72]. Tatara and Fukuyama [70] showed that, using a local spin transformation, the problem of a smooth DW with a spatially varying magnetization $\mathbf{M}(z)$ can be considered as a problem with constant magnetization, but with an additional spin-dependent gauge field. The effect of the gauge field on the cooperon is similar to that of the vector potential associated with a magnetic field, that is, the gauge field suppresses the cooperons. Thus, DWs cause suppression of the localization corrections, which leads to an increase in the conductivity in the presence of DWs. When the external magnetic field removes DWs, then the conductivity decreases, giving rise to positive magnetoresistivity. This effect should be observed in the low-temperature region, where the localization corrections are not negligible. Recently, Jonkers [81] predicted that, for a 2-D ferromagnetic wire with impurity scattering independent of the spin orientation, the suppression of WL by DWs increases with increasing impurity concentration and decreases with increasing width of the wall.

The theory described above [70, 71] was revised and further developed by Lyanda-Geller et al. [72]. They showed that, actually, the gauge field does not equivalently suppress all of the cooperon components. Strictly speaking, some components can be unaffected by this field, which means that the effect is smaller than that predicted in [70, 71].

One of the ways to quantify the effect of the domain walls on resistance of ferromagnetic films is to pattern high-quality thin (100 nm thick) epitaxially grown (110) oriented bcc Fe films [77]. These films, grown on sapphire substrates [82], display a large in-plane uniaxial magnetocrystalline anisotropy, with the easy axis parallel to the [001] direction. The films were patterned using projection optical lithography and ion milling to produce micron scale wires oriented perpendicular to the magnetic easy axis. The residual resistivity ratio of 30 and low residual resistance indicate the high crystalline quality of these films. The competition among magnetocrystalline, exchange, and magnetostatic interactions results in a pattern of regularly spaced stripe domains perpendicular to the wire axis. Variation of the wire width changes the ratio of these energies, and hence the domain size. The magnetic domain configurations were strongly affected by the magnetic history of the samples. Before imaging, the wires were magnetized to saturation with a magnetic field transverse or longitudinal to the wire axis. In the transverse case, the mean stripe domain length was 1.6 mm—much larger than in the longitudinal case, where it was 0.4 mm. The negative DW contribution to the

resistivity, which was extracted from the low-field MR of these epitaxial Fe films after taking into account the AMR contribution, was explained [77] as a possible indication for the localization corrections in the presence of DWs. However, the fact that the WL effect survived at elevated (77 K) temperatures is rather against such an explanation. A negative contribution to resistivity due to DWs was also reported by Hong and Giordano [83] in Ni wires at $T < 20$ K. Very narrow strips were patterned from Ni films evaporated onto glass substrates. The patterning was accomplished using a step-edge method [84], with typical thicknesses and widths of 200–400 Å, and sample lengths of 10 μm · km. The elastic mean-free path, estimated from low-temperature resistivity (10–20 $\mu\Omega \cdot$ cm) was comparable to, or slightly smaller than, the strip cross section. Further experimental details are given in [85]. These experiments [83], however, did not study the temperature dependence of the effect, and considered AMR as an alternative origin of the observation. In the following, we review recent experimental results on the localization corrections in antiferromagnetically coupled Fe/Cr multilayer structures in the presence of DWs [86, 87].

Antiferromagnetically (AF) coupled magnetic multilayers (MMLs) are systems of reduced magnetization, and therefore have strongly suppressed AMR. Weak pinning of DWs at high temperatures is expected to suppress the DWMR. For a fixed magnetic field, DWMR should occur at sufficiently low temperatures, where DWs become strongly pinned and their configuration is not affected by thermal fluctuations or electrical current. The GMR effect (see Section 1) in this system is dominated by realignment of the magnetization direction in adjacent magnetic layers [88]. The presence of DWs should result in a small additional in-plane MR [89]. While the GMR effect is known to saturate at low temperatures [90], the temperature dependence of DWMR is still a matter of controversy.

Epitaxial $[Fe/Cr]_{10}$ multilayers with ten bilayers were prepared in an MBE system on MgO (100)-oriented substrates held at 50 °C and covered by a 12 Å thick Cr seed layer. *In-situ* high-energy electron diffraction and *ex-situ* X-ray diffraction measurements were used to control the structural quality of the multilayers. The thickness of the Cr layers was typically 12–13 Å, which corresponds to the first antiferromagnetic peak in the interlayer exchange coupling for the Fe/Cr system [91], and gives rise to maximum GMR, which is about 20% at 300 K and 100% at 4.2 K. The antiferromagnetic fraction exceeds 80%, and the bilinear AF coupling dominates the biquadratic exchange coupling [92]. A detailed description of the sample preparation and structural characterization is given in [93].

Typical magnetic images at $T = 4.2$ K and room temperature [86, 87] reveal different irregularly shaped domains of micrometer size (which is a characteristic feature of strong AF coupling [88, 94]). The susceptibility data point toward a weak pinning of the DWs at room temperature and a strong pinning at low temperatures [87]. Figure 3a shows the temperature dependence of the electrical resistivity ρ for an $[Fe(12\ Å)/Cr]_{10}$ MML and for different magnetic fields ($|H| \leq 300$ Oe). The magnetic field was applied in the plane of the film and parallel to the current flowing along the (110) axis. For $|H| > 100$ Oe, the $\rho(T)$ dependence reveals a metallic behavior, while for $|H| \leq 100$ Oe, there is a shallow minimum in the $\rho(T)$ curves.

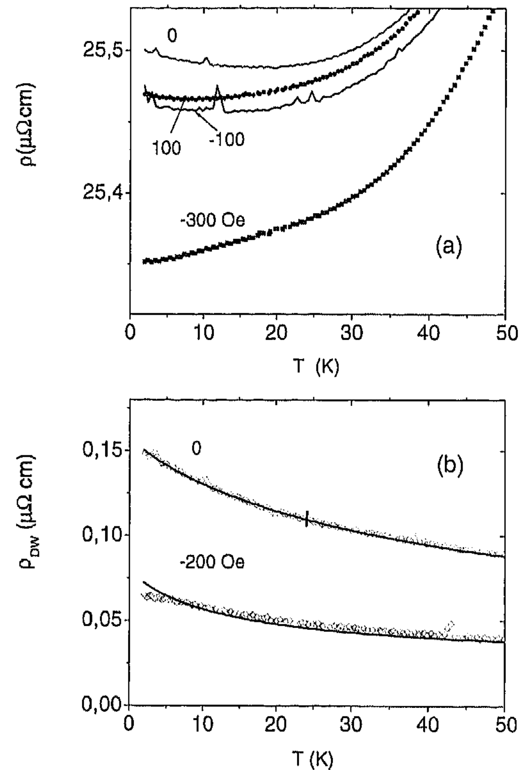

Figure 3. (a) Temperature dependence of the resistivity for $[Fe\ (12\ Å)/Cr]_{10}$ multilayer in different magnetic fields. Both the field and the current are along the (110) axis. (b) Temperature dependence of the DW contribution to the resistivity. $\rho_{DW} = \rho(T, H) - \rho(T, H_S)$ determined from the data shown in (a) for $H = 0$ and 200 Oe and $H_S = -300$ Oe. The solid lines correspond to the fits which are described in the text. Vertical bar indicates maximum influence which could cause the GMR effect as on the estimated DW contribution.

In order to separate the DW contribution to magnetoresistivity from the GMR effect, the authors of [87] estimated the DW resistivity as $\rho_{DW} = \rho(T, H) - \rho(T, H_S)$, with $|H_S| \leq 300$ Oe. Although this method may underestimate the magnetoresistivity due to DWs, because some of the domains may not be removed by the applied field H_S, it provides a possibility to determine the temperature dependence of the DW magnetoresistivity. Figure 3b shows $\rho_{DW}(T, H)$ between 1.9 and 50 K for two magnetic fields (0 and −200 Oe) and zero field when $H_S = -300$ Oe. In contrast to GMR, the DW magnetoresistivity is strongly temperature dependent at low temperatures, with no sign of saturation. The vertical bar indicates maximum influence, which could be caused by the GMR effect. This estimation was obtained from the temperature dependence of the magnetoresistivity measured for two different magnetic fields sufficiently large to remove all DWs. It is known from other measurements that, for Fe/Cr epitaxial multilayers, the GMR effect is weakly temperature dependent below 50 K; it saturates as T^2, and changes less than 7% [64]. The authors of [86, 87] also demonstrated that neither AMR (which depends on the relative orientation of the magnetization and the current I) nor the ordinary magnetoresistivity caused by the Lorentz

force (which depends on the relative orientation of I and the magnetic induction B) contributes to ρ_{DW}.

The ballistic approach to electron transport through DWs [69] requires that the mean-free path l in the epitaxial layers exceeds the DW width D, with $20 < D < 200$ nm for Fe/Cr/Fe trilayers [95]. Therefore, the condition for ballistic transport may only be fulfilled at sufficiently low temperatures [93]. Although nonballistic effects have not yet been incorporated into the theory [69], it is clear that they cannot account for the strong variation of ρ_{DW} down to 1.9 K because the mean-free path is expected to saturate at low temperatures. Moreover, the strong pinning of DWs at low temperatures [87] implies that a distortion of the current lines by domain walls [73] or a change of the DW configuration cannot account for the observed strongly temperature-dependent low-field contribution to MR in antiferromagnetically coupled magnetic multilayers.

In order to explain the strong variation of the DW magnetoresistivity at low temperatures, one has to go beyond the classical approach [69]. A certain possibility is to link the observed phenomena either to standard, disorder-related, WL effects or to scattering by isolated spins. Experimental results [86,87] are in conflict with both scenarios because the resistivity corrections with and without a magnetic field are different when a magnetic field is applied along the hard or easy axis. We note that both [70,71] and [72] theoretical works predicted a destruction of WL by DWs, although the details of the destruction mechanism are different. Direct application of these models results in a sign of the DW magnetoresistivity, which is opposite that observed experimentally. However, the sign of the localization correction may be reversed due to strong spin–orbit scattering (antilocalization) [96]. The suppression of WL corrections by DWs, predicted in [70–72], is related to the associated effective gauge potential. In contrast to the electromagnetic vector potential corresponding to an external magnetic field, the gauge field depends on the electron spin giving rise to a different influence of DWs on the different components of the cooperon [72].

Measurements of Aliev et al. [86,87] are consistent with the antilocalization effect in the absence of DWs ($H >$ 300 Oe) and its suppression in the presence of DWs ($H = 0$). It is quite natural to assume the presence of a strong SO scattering in the vicinity of the interfaces of MMLs (Rashba term [97]). In the case of strong SO scattering, MR is caused by the destruction of the singlet cooperon by the gauge field associated with DWs.

When $l \ll D$, the system can be characterized in terms of the local conductivity, which is defined as an average over distances larger than l, but smaller than D. The localization correction for a particular DW is then determined by smaller diffusive trajectories with size $L < D$, as well as by large trajectories $D < L < L_\varphi$. The localization corrections associated with the small trajectories are suppressed by the gauge field since they are located within the DW. The contribution of large trajectories to localization is small, and for strong SO scattering, the local conductivity within a DW is

$$\sigma_{\text{DW}} \simeq \sigma_0 + \frac{e^2}{4\pi^2\hbar}\left[\frac{1}{l} - \left(\frac{1}{L_{\text{DW}}^2} + \frac{1}{L_\varphi^2}\right)^{1/2}\right] \tag{12}$$

where L_{DW} is the characteristic length which is determined by the influence of the gauge potential **A**. Its magnitude can be estimated as $A \sim 1/D$, and consequently, $L_{\text{DW}} \sim D$.

Since the antilocalization correction without DW is

$$\sigma \simeq \sigma_0 + \frac{e^2}{4\pi^2\hbar}\left(\frac{1}{l} - \frac{1}{L_\varphi}\right) \tag{13}$$

one can estimate the difference in magnetoresistivity due to the DWs as

$$\sigma_{\text{DW}} - \sigma \simeq -\frac{e^2}{4\pi^2\hbar}\left[\left(\frac{1}{L_{\text{DW}}^2} + \frac{1}{L_\varphi^2}\right)^{1/2} - \frac{1}{L_\varphi}\right] \tag{14}$$

The most important feature of this evaluation of the antilocalization effects is the fact that the correction to the local conductivity is determined by the gauge field inside DWs. If the current crosses a particular DW, the correction to the local conductivity, calculated for a narrow region inside the wall, shows up in the sample resistance.

One can also estimate the influence of an external magnetic field of 300 Oe and of the internal magnetization on the localization corrections. These effects are small when the magnetic length $l_H \equiv \sqrt{\hbar c/(eH)} \gg l$. For $H = 300$ Oe, $l_H \simeq 1.4 \cdot 10^{-5}$ cm. Assuming the internal magnetic induction $B = 2$ T (a typical value for Fe), we obtain the corresponding length $l_H \simeq 1.8 \times 10^{-6}$ cm. On the other hand, the mean-free path $l \simeq 10^{-7}$ cm. Thus, both the external magnetic field and the magnetization are rather unable to effectively suppress the antilocalization corrections in these structures.

It is possible to fit the data [86,87] to Eq. (14) by assuming that L_{DW} is independent of temperature, and that the phase-breaking length L_φ varies with temperature according to a power law $L_\varphi \propto T^{-3/2}$ [12]. On the other hand, one has to introduce an additional (constant) shift of the data which takes into account the change of the resistance due to the variation of the angle between magnetic layers. It is important to note that the three different fits presented in Figure 3b correspond to the same fitting parameters, except for the parameter which describes the magnetic contrast (L_{DW}). It is found that the effective DW width L_{DW} becomes about 2.5 times larger when the magnetic field is increased from 0 to 200 Oe. Thus, the detailed analysis shows that the experiments [86,87] can be explained in terms of the suppression of antilocalization corrections by DWs.

As already mentioned, the dephasing effect may be induced, not only by the DWs, but also by the boundary magnetic field when a nonmagnetic conductor is sandwiched between two ferromagnetic layers. Tatara and Fukuyama [98] also found that spin mixing induced by SO interaction may suppress the antilocalization effect. This suppression is especially enhanced when the magnetizations of two layers are parallel.

9. LOCALIZATION CORRECTIONS TO MAGNETIC INTERACTIONS IN MULTILAYERS

The problem of magnetic interactions in magnetic multilayer structures is of high importance from the application point of view. It is closely related to the possibility of an

effective control of magnetization by an external magnetic field. Such a control is essential for the magnetoelectronic-device-based GMR effect [1,2]. During the last decade, the interlayer exchange coupling has been the subject of intensive study, both experimentally [3,4,99] and theoretically [100–104]. The main physics of the coupling is now well understood, and many experimental observations have been successfully explained by the existing theoretical models. There are several excellent review articles on the phenomenon [105–108].

The starting point of the analysis of magnetic coupling in the multilayer structures is the RKKY mechanism of *exchange interaction* between magnetic impurities in metals [109–111]. The indirect exchange interaction is mediated by itinerant electrons, which transfer the information about spin polarization from a particular impurity to another one. The key point of the RKKY mechanism is magnetic polarization of the electron gas by an impurity. Such a cloud of polarization couples to the spin of the other impurity. The effective exchange parameter varies with the distance R between magnetic impurities, and is proportional to $\cos(2k_F R)/R^3$, where k_F is the Fermi momentum of electrons in metal. Thus, the RKKY interaction changes sign with increasing R, and the corresponding oscillation period is π/k_F.

In contrast to the RKKY interaction between magnetic impurities, the magnetic interlayer coupling involves a collective interaction of a distributed magnetization within the magnetic layers. This makes the problem more complex for theoretical analysis because the application of perturbative methods is not well justified in this case. It also should be noted that both the homogeneity of the magnetization in the film plane and the finite layer thickness are of importance. This was shown in a number of works accounting for the oscillatory dependence of magnetic coupling on the layer thickness. The interlayer coupling generally depends on the spacer thickness as $J = \sum_\alpha A_\alpha \sin(k_\alpha R)/R^2$, where the index α distinguishes different oscillatory components [108].

It turns out that the above-mentioned difference in the magnetic coupling between impurities and magnetic layers is crucial for the localization effects in the magnetic interaction. The problem concerns a range of the exchange interaction related to disorder. It was suggested in the past by de Gennes [112] that an inevitable disorder should impose a damping factor $\exp(-R/l)$ on the exchange interaction between magnetic impurities, where l is the mean-free path of electrons in metal. However, a careful analysis of the interaction between magnetic impurities in disordered metals shows [113–115] that the exponential factor should be dropped in many cases. Namely, the result essentially depends on what physical quantity, determined by the interaction, is under averaging over possible realizations of the disorder.

Such a dependence is a manifestation of a nonself-averaging property of some physical quantities in the theory of disordered systems. A general rule is that we should average a physically observable quantity such as, for example, the magnitude of electric current (in many cases, it is the same as the averaging conductivity), depending on a specific realization of disorder. Correspondingly, to find the critical temperature T_c of a spin glass transition in a metallic system with magnetic impurities, we should average the expression for the transition temperature, which contains J^2. The main result of [113,114] is that, without averaging over disorder (i.e., for any specific realization of disorder), the coupling between magnetic impurities does not contain any damping factor at all. Moreover, the averaged quantity $\langle J^2 \rangle$ does not contain it either. The reason is that there is an exact compensation of the impurity contributions in diagrams describing the second power of coupling J.

However, the same approach to the theory of interlayer coupling [116] in magnetic structures with a disorder produced by nonmagnetic impurities and/or interface roughness shows that the effective interaction gains a damping factor $\exp(-R/a)$. However, the value of the interaction range a is not equal to l, and it can be considerably longer than the mean-free path of electrons in the spacer. In particular, the interfacial roughness does not change the damping factor, whereas it affects the electron mean-free path l. The nonvanishing damping factor in the interlayer coupling shows the self-averaging character of the magnetic interaction in magnetic structures, in contrast to the interaction between ions [116].

10. LOCALIZATION CORRECTIONS TO SPIN CONDUCTIVITY

The investigation of the transport properties of magnetic systems quite naturally invokes the problem of spin currents induced by some external fields (for instance, an electric field or the gradient of a magnetic field). A general theory of the spin-current response to external perturbations has been developed by Levy [117]. This approach distinguishes between the charge and spin currents, even though there is no real separation of spin and charge (both are related to the same particle). Nevertheless, in many cases, such an approach is better justified than the assumption of separated spin channels. In particular, the approach is justified for systems with large spin–orbit coupling, where a strong mixing of spin channels takes place, or for systems with strong Coulomb interaction which acts differently on the total charge and on the total spin (exchange interaction). The importance of the separation of charge and spin currents is also related to the conservation laws; there is a rigorous conservation law only for the total charge.

In the case of small perturbations, the corresponding linear response theory for the spin current can be easily developed. Such a linear response is described in terms of the spin conductivity. It can be shown that the spin conductivity and the spin diffusion coefficient obey Einstein's relation. The separation of spin and charge currents also allows us to separately study the localization effects on the spin and charge conductivities. Here, the spin conductivity is considered as a linear response of the system to an electric field. Physically, a nonvanishing spin current is possible in systems with some asymmetry in the transport properties of spin-up and spin-down electrons. The electric current in ferromagnets is usually associated with both the charge transfer and spin transfer.

The quantum corrections to spin conductivity can be derived using the same methods as in the case of corrections to charge conductivity. The localization correction to

the spin conductivity was analyzed in [118, 119], where it was shown that the correction vanishes in the absence of SO interaction. However, even if the SO interaction is present, the correction is rather small, which is due to cancellation of the contributions to spin conductivity from the spin-up and spin-down channels. It should be noted that this result is applicable to the disorder associated with localized impurity scatterers.

In the 3-D case (bulk ferromagnet), the correction to the spin conductivity has the following form:

$$\Delta\sigma_{\rm spin}^{\rm 3\text{-}D} = \frac{e}{4\pi^2\hbar}\left[\frac{1}{D_\uparrow^{1/2}}\left(\frac{1}{\tilde{\tau}_{\rm so\uparrow}} + \frac{1}{\tau_{\varphi\uparrow}}\right)^{1/2} - \frac{1}{D_\downarrow^{1/2}}\left(\frac{1}{\tilde{\tau}_{\rm so\downarrow}} + \frac{1}{\tau_{\varphi\downarrow}}\right)^{1/2}\right] \tag{15}$$

whereas in the effectively 2-D case, one finds

$$\Delta\sigma_{\rm spin}^{\rm 2\text{-}D} = -\frac{e}{4\pi^2\hbar}\ln\left[\frac{D_\uparrow(\tilde{\tau}_{\rm so\downarrow}^{-1} + \tau_{\varphi\downarrow}^{-1})}{D_\downarrow(\tilde{\tau}_{\rm so\uparrow}^{-1} + \tau_{\varphi\uparrow}^{-1})}\right] \tag{16}$$

The main contributions to the correction, originating from the shortest time τ_σ, are exactly canceled. Thus, the correction to the spin conductivity is determined by the SO relaxation time and the phase relaxation rate.

11. LOCALIZATION EFFECTS IN LOW-CARRIER-DENSITY MAGNETS

The quantum corrections to low-temperature resistivity have been studied recently in perovskite-type manganites $La_{1-x}Pb_xMnO_3$ [120] and bilayer manganites $La_{1.2}Sr_{1.8}Mn_2O_7$ [121]. The interest in these compounds is mostly related to the colossal MR (CMR), which is usually attributed to the magnetic-field-controlled scattering from localized magnetic moments. The physics of manganites is very interesting and complex because of the interplay of magnetic effects, disorder, and strong electron–electron correlations leading to Mott-type phase transitions. This results in a complex character of the temperature dependence of resistivity, with a distinguished region of prevailing scattering from magnons. Single-crystalline $La_{1.2}Sr_{1.8}Mn_2O_7$ manganites, used for studies of quantum interaction effects, were grown from sintered rods of the same nominal composition by the floating-zone method using a mirror furnace, described in detail in [122]. High-quality single crystals $La_{1-x}Pb_xMnO_3$ were grown by the flux growth using the accelerated crucible rotation technique. The detailed preparation process and composition analysis are described in [123]. A temperature dependence for $La_{1-x}Pb_xMnO_3$ perovskite manganites [120] clearly shows an increasing resistivity with decreasing temperature for $T < 50$ K. This increase obeys the low $T^{1/2}$ characteristic for quantum correction due to e–e interactions in 3-D metals or due to WL with the phase relaxation time τ_φ depending on the temperature as $\tau_\varphi \sim T^{-1/2}$ [12, 13]. The latter dependence is characteristic of the inelastic e–e scattering, which results in dephasing of the electrons. The key role of e–e interactions seems to be quite natural for these compounds, which have typical characteristics of strongly correlated electron systems. MR was found to be positive and relatively large, up to 20% at 4.2 K. The positive sign of MR has been attributed to the e–e interaction in the presence of disorder [120]. The temperature dependence of the resistivity correction for $La_{1.2}Sr_{1.8}Mn_2O_7$ was studied by Zhang et al. [121], who found the same $T^{-1/2}$ dependence. The authors proposed the explanation in the framework of WL with the dephasing time $\tau_\varphi \sim T^{-1/2}$.

Another interesting example was the observation of quantum interference effects in $Fe_{1-y}Co_ySi$ ferromagnets [124]. This system is peculiar because the two limiting compounds (for $x = 0$ and $x = 1$) are both nonmagnetic, whereas for almost all intermediate compositions, it is magnetic [125]. Polycrystalline pellets or small single crystals grown from Sb and Sn were produced from high-purity starting materials by arc melting in an argon atmosphere. Annealing of $Fe_{1-y}Co_ySi$ ($Fe_{1-x}Mn_xSi$) in evacuated quartz ampoules for 24 h at 1280 °C (four days at 1000 °C) improved the homogeneity of the samples. The linearity of the lattice constants with Co and Mn concentration indicates that Co or Mn successfully replaces Fe over the entire concentration range ($0 < x < 1$; $0 < y < 1$). Energy dispersive X-ray microanalysis confirmed the nominal concentrations. The Hall effect data established the sign and density of the carriers, and demonstrated a systematic increase in the carrier density (n) proportional to the Co and Mn concentration at small x and y [124]. It was shown that n does not change when the Curie temperature is surpassed. Spontaneous magnetization determined from the saturated value of the magnetization at high magnetic fields corresponds to approximately 1 μ_B per Co atom. These materials are highly disordered low-carrier-density ferromagnets, where the same electrons are responsible for both the magnetic properties and the electric conduction. One should note, however, the rather low coercive magnetic field, as may be determined from the analysis of the magnetization hysteresis [124]. This implies either weak ferromagnetic crystalline anisotropy and/or weak domain wall pinning. A large positive and weakly temperature-dependent MR was observed at $T < 35$ K (below the Curie temperature). Due to the similarity between the low-temperature magnetotransport for paramagnetic Al- and Mn-doped FeSi and $Fe_{1-x}Co_xSi$, the authors [124] concluded that the low-temperature MR in ferromagnetic $Fe_{1-x}Co_xSi$ is due to e–e interaction enhanced by disorder. Indeed, the dependence of the correction on the magnetic field is in good agreement with the interaction theory of magnetoconductivity in nonmagnetic 3-D systems [12, 13], provided the magnetic field is substituted by an effective field $H_{\rm eff} = H + \alpha M$, where α is a constant and M is the internal magnetization. The temperature dependence of the correction to conductivity obeys the $T^{-1/2}$ law. The temperature scaling $(\sigma - \sigma_0)/T^{\frac{1}{2}}$ versus $H_{\rm eff}/T$ has been observed for temperatures up to 100 K in some alloys, which demonstrates the strong quantum interference effects at rather high temperatures. The experimental results of the above-described works are in rough agreement with our previous analysis. Indeed, in the case of strong ferromagnets, the magnetization completely suppresses the singlet cooperons and diffusons. The effect of an external magnetic field can be seen only on the triplet

cooperons, for which the magnetic field dependence appears as in the case of nonmagnetic metals with the magnetic field H replaced by the magnetic induction B. Finally, we note that the enhanced e–e interaction effects and WL were also reported in the conductivity of ferromagnetic glasses [126, 127]. However, the presence of a minimum in resistivity at rather high temperatures (above 200 K) indicates the electron interaction with two-level systems as the most probable explanation of the effect [128].

12. COULOMB INTERACTIONS IN FERROMAGNETIC DOUBLE JUNCTIONS

When the central electrode (island) of a double-barrier junction is small, the addition of one extra electron may cost a significant amount of energy. This addition energy includes a contribution following from the quantization of the energy levels of the island, and also a term due to the electrostatic interaction of the extra electron with other electrons being on the island. These two contributions may be comparable. In a few-electron quantum dot, the discreteness is important. In metallic islands (grains) of nanometer size, on the other hand, the quantization of the energy levels is less important, and in that case, the energy related to the electrostatic interaction plays a dominant role. In the simplest case, one may approximate the electrostatic energy by a phenomenological charging energy $E_c = e^2/2C$, where C is the capacitance of the island. The charging energy defined in this way is independent of the distribution of electrons between different discrete levels. This phenomenological model describes the transport characteristics rather well for the energy relaxation time on the island smaller than the injection time (time between the following tunneling events). When the capacitance C is sufficiently small, one can then reach the regime where the charging energy E_c is larger than the thermal energy $k_B T$. If this is the case, discrete charging of the island with single electrons modifies the junction current–voltage characteristics, leading to a Coulomb blockade of the electric current below a certain threshold voltage and to characteristic Coulomb steps above the threshold [22]. When the system is in the blocked state, then the blockade can be removed by applying a gate voltage to the island. The system then acts like a transistor, in which, however, electrons are transmitted in a correlated way one by one, and therefore the device is called a single-electron transistor (SET).

There are two methods of magnetic control of the Coulomb blockade phenomena. First, one can apply a relatively strong magnetic field which, owing to the Zeeman splitting of the energy states and spin asymmetry in the density of electron states, induces a shift of the chemical potential in the ferromagnetic electrodes (external and/or central), and therefore effectively acts as a magnetic gate. This method, however, is limited to rather small charging energies and, consequently, to low temperatures (due to the small Zeeman energy) [23].

Another method of magnetic control of the Coulomb blockade effects follows from the sensitivity of the charging effects to the relative orientation of the magnetic moments of the grain (if it is magnetic) and external electrodes [129, 130]. This technique is not limited to low temperatures, and for realistic parameters, can also work at room temperatures. We will restrict our further considerations to this method and to a double junction, in which both external electrodes are ferromagnetic, while the island is nonmagnetic.

Generally, one can distinguish three relevant time scales in electronic transport through ferromagnetic (FM) or nonmagnetic (NM) double junctions: (1) spin-conserving energy relaxation time on the island τ_ϵ, (2) current injection time τ_I, and (3) spin-flip relaxation time τ_{sf}. In real systems, τ_ϵ is usually the shortest time scale, $\tau_\epsilon < 10^{-9}$ s, whereas τ_{sf} can be in the range 10^{-9}–10^{-6} s. On the other hand, for a current of 1 nA, the injection time is of the order of 10^{-9} s. Thus, the slow spin relaxation limit is experimentally accessible. Accordingly, one may assume that the shortest time scale in many systems is the spin-conserving energy relaxation time. As concerns the other two time scales, we will distinguish two regimes. The first is the slow spin relaxation regime, where the longest time scale is the spin-flip relaxation time $\tau_{sf} \gg \tau_I \gg \tau_\epsilon$. In this regime, an electron tunneling to the island relaxes to the relevant Fermi level before the next tunneling processes occur. However, the electron can preserve its spin orientation for a time much longer than the time between successive tunneling events (injection time). This means that the electrons on the island in a steady state can be described by two Fermi levels corresponding to opposite spin orientations [131–133]. The second regime is the so-called fast spin relaxation regime, where τ_{sf} becomes of the order of τ_I or even shorter. In that case, there is a common Fermi level for different spin orientations [129, 130]. In this limit, the two external electrodes become magnetically decoupled, and when the central electrode is nonmagnetic, the total current flowing through the system is independent of the magnetic configuration. In the following, we assume spin-conserving tunneling through the barriers, and define positive bias V as the one corresponding to current flowing from the left to the right (electrons flow in the opposite direction).

12.1. Limit of Continuous Density of States

Assume that the effects due to the quantization of energy levels on the island are negligible. Such an assumption is reasonable when the separation between discrete energy levels is much smaller than the charging energy, and also significantly smaller than the thermal energy $k_B T$. When the barrier resistances are larger than the quantum resistance R_q ($R_q \approx 26$ kΩ), one can use the "orthodox" tunneling theory to describe electronic transport. In the sequential tunneling regime, an electron tunnels to the island through one barrier, and later another electron leaves the island through the second barrier (or vice versa). These processes are suppressed below a certain threshold voltage, and therefore are dominant only above the first Coulomb step. The electric current I in the sequential tunneling regime can be calculated from the formula

$$I = -e \sum_N P(N) \sum_\sigma \{\Gamma^+_{l\sigma}(N) - \Gamma^-_{l\sigma}(N)\}$$
$$= e \sum_N P(N) \sum_\sigma \{\Gamma^+_{r\sigma}(N) - \Gamma^-_{r\sigma}(N)\} \qquad (17)$$

where e is the absolute value of electron charge ($e > 0$), $\Gamma^{\pm}_{\alpha\sigma}(N)$ ($\alpha = l$ for the left junction and $\alpha = r$ for the right junction) are the tunneling rates for electrons with spin σ, which tunnel to the island (+) from the lead α or back (−), whereas $P(N)$ is the probability of finding N excess electrons on the island.

The probability $P(N)$ is usually calculated from the master equation

$$\partial P(N)/\partial t = 0 = -\Gamma(N)P(N) + P(N-1)\sum_{\sigma}\Gamma^{+}_{\sigma}(N-1) + P(N+1)\sum_{\sigma}\Gamma^{-}_{\sigma}(N+1) \quad (18)$$

where $\Gamma^{\pm}_{\sigma}(N) = \Gamma^{\pm}_{l\sigma}(N) + \Gamma^{\pm}_{r\sigma}(N)$ and $\Gamma(N) = \sum_{\sigma}\{\Gamma^{+}_{\sigma}(N) + \Gamma^{-}_{\sigma}(N)\}$. From this follows that, in a steady state, the net transition rate between the states with N and $N+1$ excess electrons on the island is equal to zero, which can be used to calculate the probability $P(N)$ [134].

The transition rate $\Gamma^{+}_{r\sigma}(N)$ is given by

$$\Gamma^{+}_{r\sigma}(N) = \frac{2\pi}{\hbar}\int dE|T_{r\sigma}(E)|^2 D_{r\sigma}(E - E^{(r)}_F)D_{i\sigma}(E - E^{(i)}_{F\sigma}) \times f(E - E^{(r)}_F)[1 - f(E - E^{(i)}_{F\sigma})] \quad (19)$$

where $T_{r\sigma}(E)$ is an average transition matrix element for electronic states of energy E, while $E^{(i)}_{F\sigma}$ and $E^{(r)}_F$ are the Fermi levels, respectively, for the island and right electrode. Due to spin accumulation on the island in a general case, the Fermi level $E^{(i)}_{F\sigma}$ is spin dependent. The difference between $E^{(i)}_{F\sigma}$ and $E^{(r)}_F$ depends on the applied voltage and the number of excess electrons on the grain, and can be written as $E^{(i)}_{F\sigma} - E^{(r)}_F = E_c + \Delta E^{(i)}_{\sigma} - eV_r(N)$. Here, $E_c = e^2/2(C_l + C_r)$, and $V_r(N)$ is the potential drop at the right junction, $V_r(N) = C_l V/(C_l + C_r) - Ne/(C_l + C_r)$, with C_l and C_r the capacitances of the two junctions ($C_l + C_r = C$). Apart from this, $\Delta E^{(i)}_{\sigma}$ is a shift of the chemical potential of the grain for spin σ, which is caused by spin accumulation.

Generally, the spin dependence of the transition rates $\Gamma^{+}_{\alpha\sigma}(N)$ and $\Gamma^{-}_{\alpha\sigma}(N)$ ($\alpha = 1, 2$) follows from the spin dependence of the matrix elements, the spin dependence of the density of electron states, and the spin dependence of the Fermi level. For constant (independent of energy) matrix elements and density of states in the electrodes, the transition rate $\Gamma^{+}_{r\sigma}(N)$ can be written as

$$\Gamma^{+}_{r\sigma}(N) = \frac{1}{e^2 R_{r\sigma}}\frac{+eV_r(N) - E_c - \Delta E^{(i)}_{\sigma}}{1 - \exp\{[-eV_r(N) + E_c + \Delta E^{(i)}_{\sigma}]/kT\}} \quad (20)$$

where $R_{r\sigma}$ is the resistance of the right junction for the spin channel σ. Formulas similar to Eq. (20) also can be written for $\Gamma^{-}_{r\sigma}(N)$ and for the tunneling rates $\Gamma^{+}_{l\sigma}(N)$ and $\Gamma^{-}_{l\sigma}(N)$ through the left junction.

For arbitrary τ_{sf}, the chemical potential shifts $\Delta E^{(i)}_{\sigma}$ can be determined from the relevant balance equation which, for the case of a nonmagnetic island, takes the form

$$\frac{1}{e}(I^{(r)}_{\uparrow} - I^{(l)}_{\uparrow}) - \frac{2D}{\tau_{sf}}\Delta E^{(i)}_{\uparrow} = 0 \quad (21)$$

where $I^{(\alpha)}_{\uparrow}$ ($\alpha = l, r$) is the current of spin-up electrons through the αth junction, D is the density of electron states in the island per spin, and the condition $\Delta E^{(i)}_{\sigma} = -\Delta E^{(i)}_{-\sigma}$ was used (valid for nonmagnetic islands). The chemical potential shifts and electric current flowing through the junction have to be calculated self-consistently.

Typical transport characteristics of a double-barrier junction with a nonmagnetic island are shown in Figure 4 for both parallel and antiparallel magnetic configurations, and for the slow spin relaxation limit on the island. In both cases, the electric current is blocked below a certain threshold voltage, which is determined by the charging energy and the ratio of capacitances C_l/C_r. Current flows above the threshold voltage and a typical Coulomb staircase then can be observed. Each step corresponds to a new charge state of the island, and consequently, to a new channel for electron tunneling. The Coulomb steps are well resolved for an asymmetric junction, when the resistances of both barriers are significantly different. However, the steps of the Coulomb "staircase" above the threshold voltage are qualitatively different in the parallel and antiparallel configurations. This difference is due to spin accumulation and associated shifts of the chemical potentials. When the electrodes are of the same ferromagnetic material, there is no spin accumulation on the island in the parallel configuration, and consequently, no spin splitting of the chemical potential. Thus, the current–voltage curves in this configuration are similar to those for nonmagnetic junctions. In contrast, in the antiparallel configuration, the spin asymmetries for both junctions are different, and a nonequilibrium magnetic moment builds up on the island (spin accumulation) until the tunneling rates for a given spin orientation become equal for both junctions. The additional kinks on the I–V curve for the antiparallel configuration correspond to the local maxima of spin accumulation. Since the I–V characteristics are different in the parallel and antiparallel configurations, transition

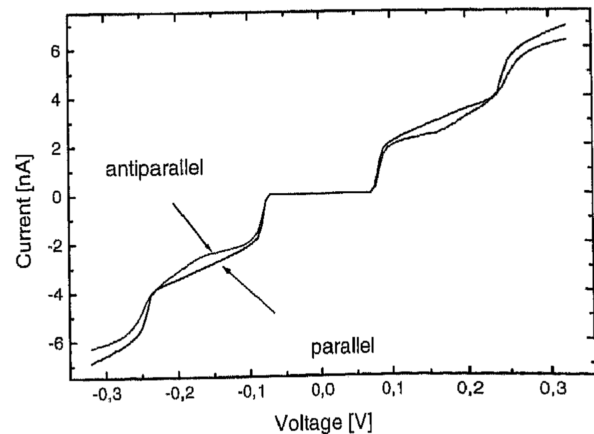

Figure 4. Typical current–voltage characteristics in the parallel and antiparallel configurations, calculated for the long spin-flip relaxation time limit. The junction consists of two identical ferromagnetic outer electrodes, two nonmagnetic barriers, and a nonmagnetic metallic central electrode. The parameters assumed are: E_c = 40 meV, kT = 1 meV, R_{1+} = 2 MΩ, R_{1-} = 0.5 MΩ, R_{2+} = 200 MΩ, R_{2-} = 50 MΩ, and $C_1/C_2 = 1$. Here, $\sigma = \pm$ corresponds to the majority (minority) electrons.

from one configuration to the other results in a nonvanishing TMR effect, which varies with the bias voltage reflecting the features in the corresponding I–V curves.

When the spin-flip relaxation time for the island becomes shorter, the TMR effect decreases. In the case of a nonmagnetic island, no TMR appears in the fast spin relaxation limit. The transition from slow to fast spin relaxation was considered in [135], where it was shown that TMR drops relatively fast to almost zero when the spin relaxation time approaches the injection time.

Sequential tunneling processes are suppressed below the threshold voltage. However, there are still processes of higher order (cotunneling), which can transport charge between the source and drain electrodes [130]. In the cotunneling processes, two tunneling events are correlated in time, and are not blocked by the charging energy. Being of higher order, they are less effective, and therefore the electric current in the cotunneling regime is smaller than in the sequential one. Close to the threshold voltage, however, both currents may be comparable.

The cotunneling processes can be calculated perturbatively. The lowest order perturbation description is valid sufficiently well below the threshold voltage. However, a more general description has been worked out, which is also valid in the transition regime. Such a description was formulated in terms of closed-time path Green functions [136] for nonmagnetic SETs. This description was extended recently to magnetic systems [137]. It includes the double-barrier cotunneling processes directly contributing to electric current, and the single-barrier cotunneling processes which—although do not contribute directly to the flowing current—give an indirect contribution via modification of the magnetic state of the island. Other cotunneling processes lead to vertex and propagator renormalization. When the spin relaxation time on the island is long, the cotunneling processes—similarly as the sequential ones—lead to spin accumulation on the island.

12.2. Role of Discreteness

When $kT \ll \Delta E$, the size quantization of energy levels on the island must be taken into account [138–140]. To describe the transport properties, the "orthodox" tunneling theory [141] was generalized by taking into account the electron spin [140]. The electric current in a stationary state is now given by the formula [140]

$$\begin{aligned} I &= -e\sum_{\sigma}\sum_{N_\uparrow,N_\downarrow} P(N_\uparrow,N_\downarrow)\{\Gamma^{+}_{l\sigma}(N_\uparrow,N_\downarrow)-\Gamma^{-}_{l\sigma}(N_\uparrow,N_\downarrow)\} \\ &= e\sum_{\sigma}\sum_{N_\uparrow,N_\downarrow} P(N_\uparrow,N_\downarrow)\{\Gamma^{+}_{r\sigma}(N_\uparrow,N_\downarrow)-\Gamma^{-}_{r\sigma}(N_\uparrow,N_\downarrow)\} \end{aligned} \quad (22)$$

where $\Gamma^{\pm}_{\alpha\sigma}(N_\uparrow, N_\downarrow)$ are the tunneling rates for electrons with spin σ tunneling to the island (+) from the lead $\alpha = l, r$ or back (−), and $P(N_\uparrow, N_\downarrow)$ is the probability to find $N_\uparrow$ and $N_\downarrow$ excess electrons on the island with the spin $\sigma = \uparrow$ and $\sigma = \downarrow$, respectively. The total number of excess electrons on the island is $N = N_\uparrow + N_\downarrow$, while its magnetic moment is determined by $M = N_\uparrow - N_\downarrow$. As before, only spin-conserving tunneling processes are taken into account in Ex. (22).

The probability $P(N_\uparrow, N_\downarrow)$ can be calculated from the following master equation [140]:

$$\begin{aligned} &\partial P(N_\uparrow, N_\downarrow)/\partial t \\ &= 0 = -[\Gamma(N_\uparrow, N_\downarrow) + \Omega_{\uparrow,\downarrow}(N_\uparrow, N_\downarrow) + \Omega_{\downarrow,\uparrow}(N_\uparrow, N_\downarrow)] \\ &\quad \times P(N_\uparrow, N_\downarrow) + \Gamma^{+}_{\uparrow}(N_\uparrow - 1, N_\downarrow)P(N_\uparrow - 1, N_\downarrow) \\ &\quad + \Gamma^{+}_{\downarrow}(N_\uparrow, N_\downarrow - 1)P(N_\uparrow, N_\downarrow - 1) + \Gamma^{-}_{\uparrow}(N_\uparrow + 1, N_\downarrow) \\ &\quad \times P(N_\uparrow + 1, N_\downarrow) + \Gamma^{-}_{\downarrow}(N_\uparrow, N_\downarrow + 1)P(N_\uparrow, N_\downarrow + 1) \\ &\quad + \Omega_{\uparrow,\downarrow}(N_\uparrow - 1, N_\downarrow + 1)P(N_\uparrow - 1, N_\downarrow + 1) \\ &\quad + \Omega_{\downarrow,\uparrow}(N_\uparrow + 1, N_\downarrow - 1)P(N_\uparrow + 1, N_\downarrow - 1) \end{aligned} \quad (23)$$

where $\Gamma^{\pm}_{\sigma}(N_\uparrow, N_\downarrow) = \sum_{\alpha=l,r}\Gamma^{\pm}_{\alpha\sigma}(N_\uparrow, N_\downarrow)$ and $\Gamma(N_\uparrow, N_\downarrow) = \sum_{\sigma}[\Gamma^{+}_{\sigma}(N_\uparrow, N_\downarrow) + \Gamma^{-}_{\sigma}(N_\uparrow, N_\downarrow)]$. The tunneling rates $\Gamma^{\pm}_{\alpha\sigma}(N_\uparrow, N_\downarrow)$ include tunneling process between the lead α and all discrete levels $E_{n\sigma}$ of the island. The Ω terms, on the other hand, take into account the spin-flip process on the island. For a nonmagnetic island, one may assume that the discrete energy levels $E_{n\sigma}$ are independent of the spin orientation. One can also simplify the description further by assuming that the levels are equally separated, with the level spacing ΔE. The tunneling rates $\Gamma^{\pm}_{\alpha\sigma}(N_\uparrow, N_\downarrow)$ can be then expressed in terms of the bare tunneling rates $\gamma^{\alpha}_{n\sigma} = \Delta E/e^2 R_{\alpha\sigma}$ [141]. When the level separation ΔE becomes of the order of $k_B T$ or larger, but still smaller than E_c, the effects due to the discrete structure become visible in the transport characteristics as additional small steps [140].

13. TRANSPORT THROUGH QUANTUM DOTS WITH ELECTRON CORRELATIONS

Further features appear when $E_c \leq \Delta E$. A limiting case is when tunneling takes place through a single discrete level. The system consisting of a single-level nonmagnetic quantum dot coupled to two ferromagnetic leads can be described by the Hamiltonian $H = H_l + H_r + H_d + H_t$, where the first two terms, H_l and H_r, describe the left and right electrodes (in the noninteracting particle approximation, for simplicity), whereas the term H_d describes the dot, and can be taken in the Hubbard form $H_d = \sum_\sigma \epsilon_d c^{+}_{\sigma} c_\sigma + U c^{+}_{\uparrow} c_\uparrow c^{+}_{\downarrow} c_\downarrow$, in which ϵ_d is the energy of the discrete level, U is the electron correlation parameter, and c^{+}_{σ} (c_σ) are the creation (annihilation) operators for the dot. The energy level ϵ_d includes the electrostatic part, $\epsilon_d = \epsilon^0_d + eU_e$, where ϵ^0_d is the level energy at zero bias, and U_e is the electrostatic potential of the dot. The last term, H_t, is the tunneling part of the Hamiltonian, where only spin-conserving tunneling processes are taken into account.

When the tunneling rates are small, the transport characteristics can be calculated within the master equation technique [142,143]. In a more general situation, such a description is not sufficient since it does not properly take into account the electron correlations on the dot. It also breaks down in the strong tunneling regime and at low temperatures, where many body effects become important and lead to the Kondo effect. A more accurate description

is based on the nonequilibrium Green's functions (NGFs) [144, 145].

The tunneling current J_σ can be calculated from the formula [144–146]

$$J_\sigma = \frac{ie}{\hbar}\int \frac{d\epsilon}{2\pi}[f_l(\epsilon) - f_r(\epsilon)]\frac{\Gamma^r_\sigma(\epsilon)\Gamma^l_\sigma(\epsilon)}{\Gamma^r_\sigma(\epsilon)+\Gamma^l_\sigma(\epsilon)} \times \left[\langle\langle c_\sigma; c^+_\sigma\rangle\rangle^r_\epsilon - \langle\langle c_\sigma; c^+_\sigma\rangle\rangle^a_\epsilon\right] \quad (24)$$

where $\langle\langle c_\sigma; c^+_\sigma\rangle\rangle^r_\epsilon$ and $\langle\langle c_\sigma; c^+_\sigma\rangle\rangle^a_\epsilon$ are the retarded and advanced Green's functions, $f_l(\epsilon)$ and $f_r(\epsilon)$ are the Fermi distribution functions for the left and right electrodes, whereas $\Gamma^l_\sigma(\epsilon)$ and $\Gamma^r_\sigma(\epsilon)$ are the contributions to the half width of the discrete level due to electron tunneling to the left and right electrodes, respectively. The formula (26) is valid when $\Gamma^l_\sigma(\epsilon)$ and $\Gamma^r_\sigma(\epsilon)$ are proportional, $\Gamma^l_\sigma(\epsilon) = \lambda\Gamma^r_\sigma(\epsilon)$.

Equations of motion for the retarded and advanced Green's functions contain the occupation numbers $n_\sigma = \langle c^+_\sigma c_\sigma\rangle$, which in turn are determined by the lesser Green's function $\langle\langle c_\sigma; c^+_\sigma\rangle\rangle^<_\epsilon$ via the formula, $n_\sigma = \int(d\epsilon/2\pi) \times \mathrm{Im}\langle\langle c_\sigma; c^+_\sigma\rangle\rangle^<_\epsilon$. Thus, to find the electric current, one needs to calculate self-consistently all of the Green's functions, occupation numbers, and the electrostatic potential. When the Kondo effect is irrelevant, the Green's functions can be calculated in the Hartree–Fock approximation.

When the temperature is sufficiently low, the Kondo resonance in the density of states is formed, which has a dramatic influence on transport through the dot. The Kondo effect occurs in quantum dots containing an odd number of electrons, and is related to screening of the dot spin by conduction electrons in the leads. This screening is a many-body effect which occurs due to exchange coupling between the electrons on the dot and in the leads. In the case of quantum dots connected to nonmagnetic leads, the Kondo effect was extensively studied in the past decade. However, some new interesting questions arise when the leads are ferromagnetic and the conduction electrons are spin polarized. Recent theoretical results show that the Kondo effect still persists in such systems, although its characteristics are significantly modified [147, 148].

14. SUMMARY

The localization and interaction corrections to electrical conductivity can be significant not only in nonmagnetic, but also in ferromagnetic disordered metals or nanoscopic structures. As ferromagnetism diminishes localization corrections (and generally suppresses the singlet cooperon leading to the absence of weak antilocalization), the interaction corrections are rather unaffected by the ferromagnetism, and therefore can be easily observed in ferromagnetic systems. The corrections are important only at relatively low temperatures. Generally, there are some experimental works which confirm the importance of the WL and e–e interaction corrections. These data were usually accounted for on the basis of the theoretical results obtained for nonmagnetic systems. Even though the physical origin of quantum corrections in ferromagnets is substantially the same as in nonmagnetic systems, there is an important difference due to the presence of internal magnetization and magnetic induction in ferromagnets.

Electron–electron interaction also leads to significant effects in ferromagnetic mesoscopic double-barrier tunnel junctions, which are also observable at high temperatures. In the case of a sufficiently large central electrode, this interaction can be described by a phenomenological charging energy. This charging energy leads to a Coulomb blockade of electric current below a certain threshold voltage, and also to Coulomb steps at higher voltages. The interplay of ferromagnetism and charging effects leads to some new features in the transport characteristics. Some of these features result from nonequilibrium spin accumulation at the small central electrode. When the central electrode is a quantum dot, the Coulomb correlation on the dot can be described in terms of the Hubbard model. Electronic transport then takes place through a small number of discrete levels (or even through a single level), which leads to additional features.

Coherent transport in the low-temperature range as well as ferromagnetic tunnel junctions (also operating at high temperature) are of potential importance for applications in magnetoelectronics and spintronics devices. The ferromagnetic systems or ferromagnetic components of a more complex device can be either metallic or semiconducting. Recently, huge efforts have been undertaken to grow ferromagnetic semiconductors with room-temperature ferromagnetism. The phenomena described in this review apply to ferromagnetic semiconductors too.

GLOSSARY

Anisotropic magnetoresistance (AMR) Magnetoresistance observed in ferromagnetic metals which depends on relative orientation of electric current and magnetization.

Anomalous hall effect (AHE) Transverse current induced by the electric field in ferromagnets in the absence of external magnetic field.

Giant magnetoresistance (GMR) Magnetoresistance in magnetic multilayer system related to the switch from antiferromagnetic to ferromagnetic ordering in magnetic layers by weak magnetic field.

Magnetic multilayers (MMLs) Alternating thin layers of magnetic and nonmagnetic metals.

Magnetoresistance (MR) Variation of the resistance of metals and semiconductors in magnetic field.

Molecular beam epitaxy (MBE) Technology of the epitaxial growth of thin films using molecular beams.

Ruderman-Kittel-Kasuya-Yosida interaction (RRKY) Magnetic interaction due to the exchange between magnetic impurities via free electron gas.

Spin–orbit interaction (SO) The interaction affecting the spin state of a particle due to its orbital motion.

Tunneling magnetoresistance (TMR) Magnetoresistance in tunneling systems with magnetic overlayers.

Weak localization (WL) Theory of weak corrections to conductivity in metals and heavily doped semiconductors induced by disorder.

ACKNOWLEDGMENTS

V. K. Dugaev is grateful to P. Bruno for many stimulating discussions. F. G. Aliev thanks R. Villar for critical reading of the manuscript. This work was supported by the Polish Committee for Scientific Research under Grants 5 P03B 091 20 and PBZ/KBN/044/P03/2001, and also by Spanish MCyT (BFM2000-0016) and CM (07N/0050/2002).

REFERENCES

1. M. N. Baibich, J. M. Broto, A. Fert, F. Nguyen van Dau, F. Petroff, P. Etienne, G. Creuzet, A. Friederich, and J. Chazelas, *Phys. Rev. Lett.* 61, 2472 (1988).
2. G. Binasch, P. Grünberg, F. Saurenbach, and W. Zinn, *Phys. Rev. B* 39, 4828 (1989).
3. P. Grünberg, R. Schreiber, Y. Pang, M. B. Brodsky, and H. Sowers, *Phys. Rev. Lett.* 57, 2442 (1986).
4. S. S. P. Parkin, N. More, and K. P. Roche, *Phys. Rev. Lett.* 64, 2304 (1990).
5. J. M. George, L. G. Pereira, A. Barthelemy, F. Petroff, L. Steren, J. L. Duvail, A. Fert, R. Loloee, P. Holody, and P. A. Schroeder, *Phys. Rev. Lett.* 72, 408 (1994).
6. J. Barnaś, A. Fuss, R. E. Camley, P. Grünberg, and W. Zinn, *Phys. Rev. B* 42, 8110 (1990).
7. W. P. Pratt Jr., S. F. Lee, J. M. Slaughter, P. A. Schroeder, and J. Bass, *Phys. Rev. Lett.* 66, 3060 (1991).
8. M. A. M. Gijs, S. K. J. Lenczowski, and J. B. Giesbers, *Phys. Rev. Lett.* 70, 3343 (1993).
9. A. Blondel, J. P. Meier, B. Doudin, and J.-Ph. Ansermet, *Appl. Phys. Lett.* 65, 3019 (1994).
10. P. W. Anderson, *Phys. Rev.* 109, 1492 (1958).
11. B. L. Altshuler, A. G. Aronov, D. E. Khmelnitskii, and A. I. Larkin, in "Quantum Theory of Solids" (I. M. Lifshits, Ed.), p. 130. Mir, Moscow, 1982.
12. P. A. Lee and T. V. Ramakrishnan, *Rev. Mod. Phys.* 57, 287 (1985).
13. B. L. Altshuler and A. G. Aronov, in "Electron-Electron Interaction in Disordered Systems" (A. L. Efros and M. Pollak, Eds.), p. 1. Elsevier, Amsterdam, 1985.
14. H. Fukuyama, in "Electron-Electron Interaction in Disordered Systems" (A. L. Efros and M. Pollak, Eds.), p. 155. Elsevier, Amsterdam, 1985.
15. G. Bergmann, *Phys. Rep.* 107, 1 (1984).
16. A. I. Larkin and D. E. Khmelnitskii, *Usp. Fiz. Nauk* 182, 536 (1982).
17. C. Van Haesendonck, L. Van den dries, Y. Bruynseraede, and G. Deutcher, *Phys. Rev. B* 25, 5090 (1982).
18. G. A. Prinz, *J. Magn. Magn. Mater.* 200, 57 (1999).
19. M. Julliere, *Phys. Lett. A* 54, 225 (1975).
20. J. S. Moodera, L. R. Kinder, T. M. Wong, and R. Meservey, *Phys. Rev. Lett.* 74, 3273 (1995).
21. M. Wilczyński and J. Barnaś, *J. Magn. Magn. Mater.* 221, 373 (2000).
22. For a review, see: "Single Charge Tunneling" (H. Grabert and M. H. Devoret, Eds.), NATO ASI Series Vol. 294. Plenum, New York, 1992.
23. K. Ono, H. Shimada, S. Kobayashi, and Y. Outuka, *J. Phys. Soc. Jpn.* 65, 3449 (1996); H. Shimada, K. Ono, and Y. Outuka, *J. Phys. Soc. Jpn.* 67, 1359 (1998).
24. S. Kobayashi, Y. Ootuka, F. Komori, and W. Sasaki, *J. Phys. Soc. Jpn.* 51, 689 (1982).
25. S. Kovayashi, F. Komori, Y. Ootuka, and W. Sasaki, *J. Phys. Soc. Jpn.* 49, 1635 (1980).
26. F. Komori, S. Kovayashi, Y. Ootuka, and W. Sasaki, *J. Phys. Soc. Jpn.* 50, 1051 (1981).
27. H. Raffy, L. Dumoulin, and J. P. Burger, *Phys. Rev. B* 36, 2158 (1987).
28. "Handbook of Mathematical Functions" (M. Abramowitz and I. A. Stegun, Eds.), Natl. Bur. Stand. (U.S.) Appl. Math. Ser. GPO, New York, 1964.
29. A. I. Larkin, *JETP Lett.* 31, 220 (1980).
30. W. W. Fuller, M. Rubinstein, S. A. Wolf, and G. A. Prinz, "Proceedings of International Conference on Localization, Interaction, and Transport Phenomena in Impure Metals," Braunschweig, 1984, Vol. 135.
31. M. Rubinstein, F. J. Rachford, W. W. Fuller, and G. A. Prinz, *Phys. Rev. B* 37, 8689 (1988).
32. H. Jaffres, L. Ressier, J. P. Peyrade, A. R. Fert, P. Gogol, A. Thiaville, A. Schuchl, and F. Nguyen Van Dau, *J. Appl. Phys.* 84, 4375 (1998).
33. G. A. Prinz and J. J. Krebs, *Appl. Phys. Lett.* 39, 397 (1981).
34. G. A. Prinz, J. M. Ferrari, and M. Goldenberg, *Appl. Phys. Lett.* 40, 1551 (1982).
35. M. Aprili, J. Lesueur, L. Dumoulin, and P. Nédellec, *Solid State Commun.* 102, 41 (1997).
36. V. K. Dugaev and J. Barnaś, *Europhys. Lett.* 54, 105 (2001).
37. V. K. Dugaev, P. Bruno, and J. Barnaś, *Phys. Rev. B* 64, 144423 (2001).
38. V. K. Dugaev and J. Barnaś, *Physica* E12, 391 (2002).
39. A. Kawabata, *Solid State Commun.* 34, 431 (1980).
40. G. Tatara and B. Barbara, *Phys. Rev.* 64, 172408 (2001).
41. B. L. Altshuler, A. G. Aronov, and B. Z. Spivak, *JETP Lett.* 33, 94 (1981).
42. A. G. Aronov and Yu. V. Sharvin, *Rev. Mod. Phys.* 59, 755 (1987).
43. F. G. Aliev, E. Senaeve, and Ch. Van Haesendonck (unpublished).
44. S. Kasai, T. Niiyama, E. Saitoh, and H. Miyajima, *Appl. Phys. Lett.* 81, 316 (2002).
45. F. G. Aliev, E. Kunnen, K. Temst, K. Mae, G. Verbanck, J. Barnaś, V. V. Moshchalkov, and Y. Bruynseraede, *Phys. Rev. Lett.* 78, 134 (1997).
46. F. G. Aliev, V. V. Moshchalkov, and Y. Bruynseraede, *Phys. Rev. B* 58, 3625 (1998).
47. J. Fassbender, U. May, B. Schirmer, R. M. Jungblut, B. Hillebrands, and G. Güntherodt, *Phys. Rev. Lett.* 75, 4476 (1995).
48. W. Weber, C. H. Back, A. Bischof, Ch. Würsch, and R. Allenspach, *Phys. Rev. Lett.* 76, 1940 (1996).
49. J. Camarero, T. Graf, J. J. de Miguel, R. Miranda, W. Kuch, M. Zharnikov, A. Dittschar, C. M. Schneider, and J. Kirschner, *Phys. Rev. Lett.* 76, 4428 (1996).
50. M. Jalochowski and E. Bauer, *Phys. Rev. B* 37, 8622 (1988).
51. Yu. A. Bychkov and E. I. Rashba, *J. Phys.* C17, 6093 (1984).
52. G. Dresselhaus, *Phys. Rev.* 100, 580 (1955).
53. "The Hall Effect and Its Applications" (C. L. Chien and C. R. Westgate, Eds.). Plenum, New York, 1980.
54. A. Crépieux and P. Bruno, *Phys. Rev. B* 64, 014416 (2001).
55. G. Bergmann and F. Ye, *Phys. Rev. Lett.* 67, 735 (1991).
56. G. Bergmann, *Phys. Rev. B* 7, 4850 (1973).
57. A. Langenfeld and P. Wölfle, *Phys. Rev. Lett.* 67, 739 (1991).
58. V. K. Dugaev, A. Crépieux, and P. Bruno, *Phys. Rev. B* 64, 104411 (2001).
59. A. Crépieux, J. Wunderlich, V. K. Dugaev, and P. Bruno, *J. Magn. Magn. Mater.* 242–245, 464 (2002).
60. V. K. Dugaev, A. Crépieux, and P. Bruno, *J. Magn. Magn. Mater.* 240, 159 (2002).
61. H. Fukuyama, *J. Phys. Soc. Jpn.* 54, 2092 (1985).
62. A. Singh and E. Fradkin, *Phys. Rev. B* 35, 6894 (1987).
63. Y. B. Kim and A. J. Millis, *Phys. Rev. B* 67, 085102 (2003).
64. F. G. Aliev, V. V. Moshchalkov, and Y. Bryunseraede, *Phys. Rev. Lett.* 81, 5884 (1998).
65. S. A. Grigera, R. S. Perry, A. J. Schofield, M. Chiao, S. R. Julian, G. G. Lonzarich, S. I. Ikeda, Y. Maeno, A. J. Millis, and A. P. Mackenzie, *Science* 294, 329 (2001).
66. P. B. Allen, H. Berger, O. Chauvet, L. Forro, T. Jarlborg, A. Junod, B. Revaz, and G. Santi, *Phys. Rev. B* 53, 4393 (1996).
67. K. Ishida, H. Mukuda, Y. Kitaoka, K. Asayama, Z. Q. Mao, Y. Mori, and Y. Maeno, *Nature* 396, 658 (1998).

68. R. S. Perry, L. M. Galvin, S. A. Grigera, L. Capogna, A. J. Schofield, A. P. Mackenzie, M. Chiao, S. R. Julian, S. I. Ikeda, S. Nakatsuji, Y. Maeno, and C. Pfleiderer, *Phys. Rev. Lett.* 86, 2661 (2001).
69. J. B. A. N. van Hoff, K. M. Schep, A. Braats, G. E. W. Bauer, and P. J. Kelly, *Phys. Rev. B* 59, 138 (1999).
70. G. Tatara and H. Fukuyama, *Phys. Rev. Lett.* 78, 3773 (1997).
71. G. Tatara, *Int. J. Mod. Phys.* B15, 321 (2001).
72. Yu. Lyanda-Geller, I. L. Aleiner, and P. M. Goldbart, *Phys. Rev. Lett.* 81, 3215 (1998).
73. L. Berger, *J. Appl. Phys.* 49, 2156 (1978).
74. K. Hong and N. Giordano, *Phys. Rev. B* 51, 9855 (1995).
75. J. F. Gregg, W. Allen, K. Ounadjela, M. Viret, M. Hehn, S. M. Thompson, and J. M. D. Coey, *Phys. Rev. Lett.* 77, 1580 (1996).
76. P. M. Levy and S. Zhang, *Phys. Rev. Lett.* 79, 5110 (1997).
77. U. Rüediger, J. Yu.S. Zhang, A. D. Kent, and S. S. P. Parkin, *Phys. Rev. Lett.* 80, 5639 (1998).
78. S. Gider, B. U. Runge, A. C. Marley, and S. S. P. Parkin, *Science* 281, 797 (1998).
79. U. Rüediger, J. Yu, L. Thomas, S. S. P. Parkin, and A. D. Kent, *Phys. Rev. B* 59, 11914 (1999).
80. M. Viret, Y. Samson, P. Warin, A. Marty, F. Ott, E. Søndergård, O. Klein, and C. Fermon, *Phys. Rev. Lett.* 85, 3962 (2000).
81. P. A. E. Jonkers, *J. Magn. Magn. Mater.* 247, 178 (2002).
82. A. D. Kent, U. Ruediger, J. Yu, S. Zhang, P. M. Levy, and S. S. P. Parkin, *IEEE Trans. Magn.* 34, 900 (1998).
83. K. Hong and N. Giordano, *J. Phys.: Cond. Matter* 10, L401 (1998).
84. D. E. Pober, M. D. Feuer, and N. Giordano, *Appl. Phys. Lett.* 37, 94 (1980).
85. K. Hong and N. Giordano, *Phys. Rev. B* 51, 9855 (1995).
86. F. G. Aliev, R. Schad, Y. Bruynseraede, and R. Villar, *Physica* B284–288, 1243 (2000).
87. F. G. Aliev, R. Schad, A. Volodin, K. Temst, C. Van Haesendonck, Y. Bruynseraede, I. Vavra, V. K. Dugaev, and R. Villar, *Europhys. Lett.* 63, 888 (2003).
88. A. Fert, P. Grünberg, A. Barthélémy, F. Petroff, and W. Zinn, *J. Magn. Magn. Mater.* 140–144, 1 (1995).
89. S. Zhang and P. M. Levy, *Phys. Rev. B* 50, 6089 (1994).
90. J. E. Mattson, M. E. Brubaker, C. H. Sowers, M. Conover, Z. Qiu, and S. D. Bader, *Phys. Rev. B* 44, 9378 (1991).
91. S. S. P. Parkin, *Phys. Rev. Lett.* 71, 1641 (1993).
92. J. C. Slonczewski, *Phys. Rev. Lett.* 67, 3172 (1991).
93. R. Schad, P. Beilen, G. Verbanck, V. V. Moshchalkov, Y. Bruynseraede, H. E. Fisher, S. Lefebvre, and M. Bessiere, *Phys. Rev. B* 59, 1240 (1999).
94. M. Rührig, R. Schäfer,A. Hubert, R. Mosler, J. A. Wolf, S. Demokritov, and P. Grünberg, *Phys. Status Solidi* A125, 635 (1991).
95. C. M. Schmidt, D. E. Bürgler, D. M. Schaller, F. Meisinger, and H.-J. Güntherodt, *Phys. Rev. B* 60, 4158 (1999).
96. W. Knap, C. Skierbiszewski, A. Zduniak, E. Litwin-Staszewska, D. Bertho, F. Kobbi, J. L. Robert, G. E. Pikus, F. G. Pikus, S. V. Iordanskii, V. Mosser, K. Zekentes, and Yu. B. Lyanda-Geller, *Phys. Rev. B* 53, 3912 (1996).
97. Yu. A. Bychkov and E. I. Rashba, *J. Phys.* C17, 6093 (1984).
98. G. Tatara and H. Fukuyama, *J. Phys. Soc. Jpn.* 69, 2407 (2000).
99. S. S. P. Parkin, *Phys. Rev. Lett.* 67, 3598 (1991).
100. D. M. Edwards, J. Mathon, R. B. Muniz, and M. S. Phan, *Phys. Rev. Lett.* 67, 493 (1991).
101. P. Bruno and C. Chappert, *Phys. Rev. Lett.* 67, 1602 (1991); *Phys. Rev. Lett.* 67, 2592 (1991).
102. J. Barnaś, *J. Magn. Magn. Mater.* 111, L215 (1992).
103. M. D. Stiles, *Phys. Rev. B* 48, 7238 (1993).
104. P. Bruno, *Phys. Rev. B* 52, 411 (1995).
105. A. Fert and P. Bruno in "Ultrathin Magnetic Structures" (B. Heinrich and J. A. C. Bland, Eds.), Vol. 2, p. 82. Springer, Berlin, 1994.
106. P. Bruno, *J. Phys.: Cond. Matter* 11, 9403 (1999).
107. J. Kudrnovský, V. Drchal, I. Turek, P. Bruno, P. Dederichs, and P. Weinberger in "Electronic Structure and Physical Properties of Solids" (H. Dreyssé, Ed.), p. 313. Springer, Berlin, 2000.
108. P. Bruno, in "Magnetism: Molecules to Materials, III, Nanosized Magnetic Materials" (J. S. Miller and M. Drillon, Eds.). Wiley-VCH, Weinheim, 2002.
109. M. A. Ruderman and C. Kittel, *Phys. Rev.* 96, 99 (1954).
110. T. Kasuya, *Prog. Theor. Phys.* 16, 45 (1956).
111. K. Yosida, *Phys. Rev.* 106, 893 (1957).
112. P.-G. de Gennes, *J. Phys. Radium* 23, 630 (1962).
113. A. Yu. Zyuzin and B. Z. Spivak, *JETP Lett.* 43, 234 (1986).
114. L. N. Bulaevski and S. V. Panyukov, *JETP Lett.* 43, 240 (1986).
115. A. Jagannathan, E. Abrahams, and M. J. Stephen, *Phys. Rev. B* 37, 436 (1988).
116. P. M. Levy, S. Maekawa, and P. Bruno, *Phys. Rev.* 58, 5588 (1998).
117. P. M. Levy, *Solid State Phys.* 47, 367 (1994).
118. V. K. Dugaev, P. Bruno, and J. Barnaś, *J. Magn. Magn. Mater.* 240, 200 (2002).
119. V. K. Dugaev, P. Bruno, and J. Barnaś, *J. Magn. Magn. Mater.* 242–245, 461 (2002).
120. P. Chen, D. Y. Xing, and Y. W. Du, *Phys. Rev. B* 64, 104402 (2001).
121. C. L. Zhang, X. J. Cheng, C. C. Almasan, J. S. Gardner, and J. L. Sarrao, *Phys. Rev. B* 65, 134439 (2002).
122. N. O. Moreno, P. G. Pagliuso, C. Rettori, J. S. Gardner, J. L. Sarrao, J. D. Thompson, D. L. Huber, J. F. Mitchell, J. J. Martinez, and S. B. Oseroff, *Phys. Rev. B* 63, 174413 (2001).
123. B. X. Gu, S. Y. Zhang, H. C. Zhang, and B. G. Shen, *J. Magn. Magn. Mater.* 204, 45 (1999).
124. N. Manyala, Y. Sidis, J. F. Di Tusa, G. Aeppli, D. P. Young, and Z. Fisk, *Nature* 404, 581 (2000).
125. J. E. Di Tusa et al., *Phys. Rev. Lett.* 78, 28431 (1997).
126. P. D. Babu, S. N. Kaul, L. F. Barquin, and J. C. Gomez Sal, *J. Magn. Magn. Mater.* 140–144, 295 (1995).
127. L. F. Barquin, J. C. Gomez Sal, P. D. Babu, and S. N. Kaulm, *J. Magn. Magn. Mater.* 133, 82 (1994).
128. R. W. Cochrane, R. Harris, J. O. Ström-Olson, and M. J. Zuckermann, *Phys. Rev. Lett.* 35, 676 (1975).
129. J. Barnaś and A. Fert, *Phys. Rev. Lett.* 80, 1058 (1998).
130. S. Takahashi and S. Maekawa, *Phys. Rev. Lett.* 80, 1758 (1998).
131. J. Barnaś and A. Fert, *Europhys. Lett.* 44, 85 (1998).
132. A. Brataas, Yu. V. Nazarov, J. Inoue, and G. E. W. Bauer, *Phys. Rev. B* 59, 93 (1999).
133. A. N. Korotkov and V. I. Safarov, *Phys. Rev. B* 59, 89 (1999).
134. M. Amman, R. Wilkins, E. Ben-Jacob, P. D. Maker, and R. C. Jaklewic, *Phys. Rev. B* 43, 1146 (1991).
135. J. Barnaś and A. Fert, *J. Magn. Magn. Mater.* 192, L 391 (1999).
136. H. Schoeller and G. Schön, *Phys. Rev. B* 50, 18436 (1994).
137. J. Martinek, J. Barnaś, S. Maekawa, H. Schöller, and G. Schön, *Phys. Rev. B* 66, 014402 (2002).
138. D. C. Ralph, S. Gueron, C. T. Black, and M. Tinkham, *Physica* B280, 420 (2000).
139. A. Brataas, Yu.V. Nazarov, J. Inoue, and G. E. W. Bauer, *Eur. Phys. J.* B9, 421 (1999).
140. J. Barnaś, J. Martinek, G. Michałek, B. R. Bułka, and A. Fert, *Phys. Rev. B* 62, 12363 (2000).
141. C. W. J. Beenakker, *Phys. Rev. B* 44, 1646 (1991).
142. B. R. Bułka, *Phys. Rev. B* 62, 1186 (2000).
143. W. Rudziński and J. Barnaś, *Phys. Rev. B* 64, 085318 (2001).
144. A. P. Jauho, N. S. Wingreen, and Y. Meir, *Phys. Rev. B* 50, 5528 (1994).
145. C. Niu, L. Liu, and T. Lin, *Phys. Rev. B* 51, 5130 (1995).
146. R. Świrkowicz, J. Barnaś, and M. Wilczyński, *J. Phys.: Cond. Matter* 14, 2011 (2002).
147. N. Sergueev, Q. Sun, H. Guo, B. G. Wang, and J. Wang, *Phys. Rev. B* 65, 165303 (2002).
148. J. Martinek, Y. Utsumi, H. Imamura, J. Barnaś, S. Maekawa, J. König, and G. Schön, *Phys. Rev. Lett.* 91, 127203 (2003).